9

Edge Enhancement Computed Tomography

Cruz Meneses-Fabian, Gustavo Rodriguez-Zurita, and Areli Montes-Pérez
Benemérita Universidad Autónoma de Puebla,
Facultad de Ciencias Físico-Matemáticas, Puebla,
México

1. Introduction

The term tomography comes from the Greek words *tomos*, which means to cut or to divide, and graphos, which is a graphic representation. Thus, tomography is a technique aimed to obtain a cut section (a slice) image of an object. This technique is extensively used in Medicine, Astrophysics, Archaeology, Biology, Geophysics, Oceanography, Material Sciences, and other scientific disciplines. Although cut sections can be obtained using several alternative or possible schemes, many of them are based on a mathematical procedure called tomographic reconstruction [Deans, 1983]. The mathematical formulae that are used to reconstruct 2D slices from several 1D so called projections were developed by the Austrian mathematician Johann Radon [1887-1956] for slices with no particular symmetry. His work were not widely known and it was rediscover in connection with radar and X-ray applications X-ray equipment was not able to make several cross-sections, neither were there the computers with the necessary capacity that is required for the automatic calculations. In order to apply them to Medicine, it was necessary to wait until enough computer power was developed. It was also required the equipment able to make several axial images separated by small distances, to electronically store the results, and finally to analyze them. All this was done separatelly by A. M. Cormack and G. H. Hounsfield in the 70´s [Byer & Garbuny, 1973]. The computerized optical tomography (OT) of X rays, substituting X rays by visible light, was born as an extension of the Computerized Tomography (CT) of X rays. The CT is considered as an non-invasive method, which make possible the cross section of objects or bodies, which have certain internal properties, without having to cut through them o to damage the sample. Basically, it consists of the sequential detection of the changes suffered by some wave when it travels through a slice with different projection angles [Byer & Shepp, 1979] and to obtain the information with adequate techniques of inversion and reconstruction algorithms [Kak & Slaney, 1987].
The radiation source is found in the visible range of the electromagnetic spectrum, and the object that will be analyzed has transparency characteristics [Byer & Shepp, 1979] in which it is possible to observe at least one of the possible effects, such as changes in the polarization, absorption, diffraction [Brown, 1966] [Wolf, 1969], refraction, birefringence, phase, etc. This paper is focused on the analysis of transparent objects that present phase effects only.
In this context, the analysis is begun considering a probe that travels as a plane wave, or in interpretative terms, as a set of parallel rays. Afterwards, the action exerted on the object after crossing is considered indifferent respect to its path, but it is affected in its amplitude and/or phase. This type of interaction is known as refractionless limit (diffractionless, no polarization

changes, no dispersion, etc.), and it is known as parallel ray tomography [Stanley, 1981]. Thus, the Radon transform is simplified and reduced to projected path integrals or to the central theorem of the Fourier transform [Stanley, 1981]. It is noteworthy that this type of approximation can be used in several applications, such as X-ray tomography [Stanley, 1981], where the amplitude of an X-ray is absorbed by the human body without deviating significantly in its path; positron-emission tomography [Kak, 1979], in which a radioactive isotope that is inside the body generates a pair of high energy particles whose paths are straight lines; optical tomography of phase objects [Byer, 1979], where thin objects in phase or absorption are considered [Brown, 1966]; and there are also interferometric techniques of spatial filtering that have been suggested [Rodríguez-Zurita *et al.,* 2005], in which a phase operation is made and a modification over the reconstruction is obtained [Philipp, *et. al*., 1993]. There are also studies of thick phase objects, but it is necessary to make a correction of the projections before applying the reconstruction algorithm [Oppenheim, *et. al*., 1973].

It is important to note that in the discussion mentioned before, it is generally assured that the image reconstruction shows information of the slice of the object under consideration. Nevertheless, in some specific cases, it can result of interest to know only the interface line that divides two media, in which a technique that reconstructs images with enhanced edges is useful.

This is particularly true for phase objects, where the detection of phase is an issue to be solved in the first place. This can be done with interferometry, or by optical derivatives, for example. In either case, an inversion procedure is needed in order to quantitatively recover the phase distribution, such as determination of the inverse tangent for the first example, or an integration for the second example. But techniques rendering edge-enhancement of phase can permit qualitative edge visualization of phase slices without such an inversion stage. This would be also true for optical amplitude derivatives, of course, but simpler schemas are possible with similar results. Hilbert transform filtering is one of them.

In this chapter, a mathematical model is described in order to obtain the reconstruction of tomographic images with enhanced edges, and there is an experimental implementation shown which is applied to optical tomography of phase objects. In the first place, there is a proof that the mathematical model is based on the establishment of the relation existent between the Radon transform (RT) and the 2-D directional Hilbert transform (HT). Afterwards, there is a description of the experimental possibility, beginning with the relation existent between the projection and the phase of the optical wave when it transverses a thin phase object, continuing with a description of the optical image-forming system 4*f* in order to obtain the HT of the optical field that is produced after crossing the object [Meneses-Fabian, 2011]. Finally, there is a description of the theoretical relationship between the experimental procedures used to obtain the image reconstruction with their enhanced edges in a directional manner whose mathematical expression accepts the directional HT of the object slice as such, and whose direction can be selected with the position of the filter in the Fourier plane of the 4*f* system respect to the projection angle [Montes-Perez *et. al.,* 2011]. Moreover, the possibility of image reconstruction with isotropic edge-enhancement is shown [Montes-Perez *et. al.,* 2011]

2. Parallel-ray tomography and the Radon transform

In tomography, the probe must be able to cross the sample and carry the information of the structure to the outside. The action exerted upon the object due to the interaction with the medium is known as the projection or profile $\check{f}$ and the predominant physical property in

the sample is denoted by the function *f*. This physical effect can be mathematically related with the Radon transform [Deans, 1983] by

$$\overset{\vee}{f} = \Re\{f\}, \tag{1}$$

where $\Re\{\cdots\}$ denotes the RT operator. Since the profile is the physical quantity that can be measured experimentally, the inverse problem consists of knowing *f* from the projections $\overset{\vee}{f}$, which implies the establishment of an inverse transform relationship.
Specifically, considering only one ray of the test probe that is crossing the sample, the path that it describes in the object can be affected in its direction, and this deviation can be caused by the effects of the refraction, but in any case, the path must follow a geodesic, because the ray will follow the path in the minimum time. Therefore, the Radon transform is described by a path integral,

$$\overset{\vee}{f} = \Re\{f\} = \int_C f dl, \tag{2}$$

where C represents the geodesic path of the ray, and *dl* is an arc differential over *C*. In this study, we will only analyze the particular case in which the geodesic is a straight line and when the lines contained in the probe are parallel, so we be discussing parallel ray tomography, and unless mentioned otherwise in this chapter, we will always refer to this type of tomography. In the experimental context, the parallel-ray tomography can be obtained when there is a medium in which the sample is immersed is very similar respect to the test object. This effect is known as refractionless limits, and there are sever examples of test probes that satisfy this condition: the X-rays that cross the human body [Bates & Peters, 1983], the positrons that emerge from an animal due to a radioactive isotope that has been introduced into it [Kak, 1979], or a light wave crossing a phase object that has been submerged in oil to equalize de refraction index [Goodman, 1985].
This discussion is focused on the study of only one slice of the object. The retrieval of the construction of a volume can be done making cuts from different positions and afterwards interpolating this set of reconstructions [Deans, 1983]. This is the reason why the definition of the Radon transform in a plane is stated in the following form:
Definition: Consider the coordinates (x, y) as points in the plane and an arbitrary function f which is defined in a domain *D* of R^2. If *L* is a straight line in the plane, then the path defined by the projection or the line integral of *f* over all the possible lines *L* is the Radon transform of *f*. In other words,

$$\overset{\vee}{f} = \Re\{f\} = \int_L f(x, y) dl, \tag{3}$$

where *dl* is a differential element of length along *L*, as shown in Fig. 1. The domain *D* can include the entire plane or it can be some region. If the Radon transform exists for every possible line *L* in the domain *D*, *f* must be continuous. Fig. 1 shows a straight line characterized by its distance from the origin and the angle that it forms with the horizontal axis, so the equation of the line *L* is given in terms of p and ϕ by the following expression:

$$p = x\cos\phi + y\sin\phi \tag{4}$$

the points (x,y) that satisfy (4) are all the points that lie along the straight line L. Rotating the reference system by an angle ϕ, where $(p,p_\perp)$ are the rotated axes, then p is given by Eq. (4) and $p_\perp$ is given by

$$p_\perp = -x\sin\phi + y\cos\phi \tag{5}$$

In the rotated system, the result is that the line L is described by $p = K$, where K is constant. Therefore, $dl = dp_\perp$ is always parallel to $p_\perp$, which indicates the propagation direction of the probe. This point of view is useful when it is necessary to numerically implement the Radon transform.

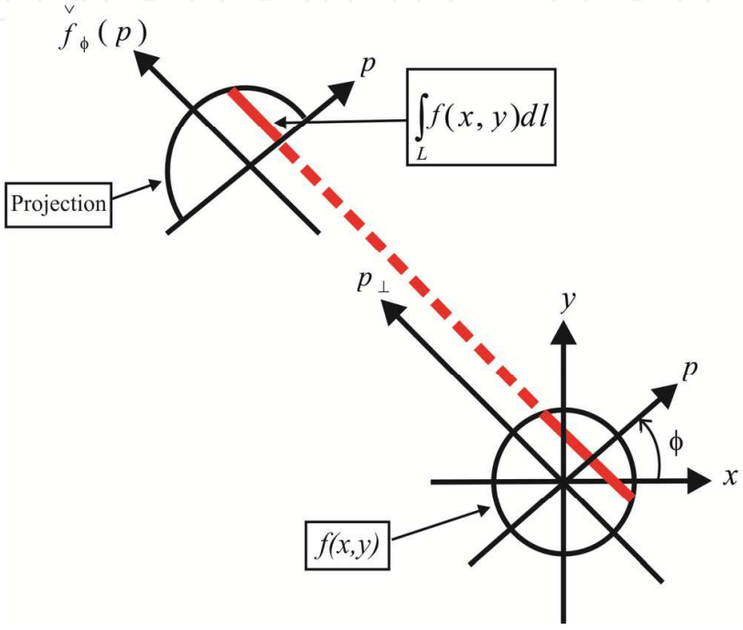

Fig. 1. The set of all the projections for every angle constitute the Radon transform.

The line L expressed in Eq. (4) can be used to rewrite the line integral described in (3) using the following equation,

$$\check{f}(p,\phi) = \Re\{f(x,y)\} = \int_{-\infty}^{\infty}\int_{-\infty}^{\infty} f(x,y)\delta(p - x\cos\phi - y\sin\phi)dxdy\,, \tag{6}$$

where $\check{f}(p,\phi)$ is the RT, the coordinates (p,ϕ) are the points that lie in the Radon space, where each point defines a line in the object space, and this point has a value given by the integral of the function $f(x,y)$ through this line. The argument of the Dirac delta function restricts the integral in the plane to the line L. The Dirac delta function selects the line $p = x\cos\phi + y\sin\phi$ from the rest of the points in the $\Re^2$ space. In this manner, the Radon transform has been defined over all the $\Re^2$ .space.

When ϕ remains constant and p is varied over all its possible values, the integral stated in Eq. (6) becomes a special case

$$\check{f}_\phi(p) = \Re_\phi\{f(x,y)\} = \int_{-\infty}^{\infty}\int_{-\infty}^{\infty} f(x,y)\delta(p - x\cos\phi - y\sin\phi)dxdy\,, \tag{7}$$

which is a sample of the RT, and it is an one-dimensional function of the variable p known as the parallel projection of the function $f(x,y)$ at an angle ϕ, p is the projection variable, and ϕ is the projection angle. Fig. 2 shows three parallel projections $\overset{\vee}{f}_{\phi}(p)$ at different projection angles.

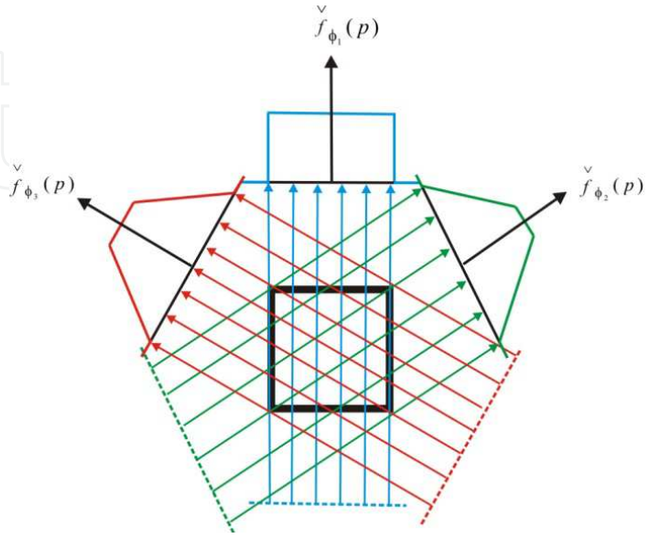

Fig. 2. Parallel projections are taken by measuring a set of parallel rays for three projection angles.

3. Properties of parallel projections

The RT defined in the last section can be extended to R^n. If the reader is interested, he can review the references [Bates & Peters, 1983], and this can also be generalized to any probe the test probe follows through the medium. In this case, the reader can review [Bates & Peters, 1983]. It is interesting to note that the RT and the projection have important properties, which can be stated as follows:

1. They are periodic from 0 to 2π.
2. They are symmetric respect to π.
3. The zero-momentum of the Radon transform is constant for any projection angle.

These properties are necessary to be sure that the Radon inverse and the unicity of the function $f(x,y)$ exist univocally in a semiperiod $\phi \in (0,\pi)$.

3.1 Proof of the properties

First property: Periodicity with a period of 2π, $\overset{\vee}{f}_{\phi+2\pi}(p) = \overset{\vee}{f}_{\phi}(p)$. The proof is trivial.

Second property: Symmetry respect to a half period π, $\overset{\vee}{f}_{\phi+\pi}(p) = \overset{\vee}{f}_{\phi}(-p)$. In this case, in order to prove it, it is only necessary to substitute $\phi = \phi + \pi$ in Eq. (7):

$$\begin{aligned}\overset{\vee}{f}_{\phi+\pi}(p) &= \int_{-\infty}^{\infty}\int_{-\infty}^{\infty} dxdyf(x,y)\delta[p - x\cos(\phi+\pi) - y\sin(\phi+\pi)] \\ &= \int_{-\infty}^{\infty}\int_{-\infty}^{\infty} dxdyf(x,y)\delta[p + x\cos\phi - y\sin\phi]\end{aligned}, \tag{8.1}$$

$$\begin{aligned} &= \int_{-\infty}^{\infty}\int_{-\infty}^{\infty} dxdyf(x,y)\delta[(-p)-x\cos\phi-y\sin\phi] \\ &= \overset{\vee}{f}_{\phi}(-p) \end{aligned} \tag{8.2}$$

which proves the property.

Third property: The property that the area is constant for every projection, which is every general, and is related with the zero-momentum of the RT defined as the integral of a tomographic projection $\int_{-\infty}^{\infty} dp\,\overset{\vee}{f}_{\phi}(p)$, which represents the probe as it is crossing the sample.

Substituting Eq. (7), it is possible to prove that:

$$\int_{-\infty}^{\infty} dp\,\overset{\vee}{f}_{\phi}(p) = \int_{-\infty}^{\infty} dp \int_{-\infty}^{\infty}\int_{-\infty}^{\infty} f(x,y)\delta(p-x\cos\phi-y\sin\phi)dxdy$$

$$\begin{aligned} &= \int_{-\infty}^{\infty}\int_{-\infty}^{\infty} f(x,y)dxdy \int_{-\infty}^{\infty} dp\delta(p-x\cos\phi-y\sin\phi) \\ &= \int_{-\infty}^{\infty}\int_{-\infty}^{\infty} f(x,y)dxdy \qquad , \\ &= \Im\{f(x,y)\}_{\mu=\nu=0} = \tilde{f}(0,0) \end{aligned} \tag{9}$$

which is the volume under the function $f(x,y)$, or the value of (0,0) order of its bidimensional Fourier-transform (FT) $\tilde{f}(0,0)$. The volume of $f(x,y)$ does not depend on ϕ. Therefore, the zero-order $\tilde{f}(0,0)$ is the only common point of the FT (one-dimensional, from p to w) of every projection, so it has to have the same value, not depending on ϕ. Interpreting the area of every projection, which must have the same value, notwithstanding the angle of incidence on the object. It is suggested that if this were carried to the expermental area, this property can be useful as a criterion for discarding experimental data if it is contradicted [Ornelas-Rodríguez *et al.,* 1999]. This property is also useful in the design of reconstruction algorithms based on iterative and/or statistical methods [Kak & Slaney, 1987].

3.2 Central slice Fourier theorem

The central slice Fourier theorem, also known as the projection theorem, describes the relation between the RT and the FT of a function. This relationship is the cap stone of parallel projection tomography, because it is the fundamental bridge to find the inverse RT and to theoretically make possible the retrieval of the internal information of the sample. The projection theorem predicts in what measure can a parallel projection to the angle ϕ can be used in the retrieval of the internal information of the object.

We begin by defining the bidimensional Fourier transform of the object function as

$$\tilde{f}(\mu,\nu) = \int_{-\infty}^{\infty}\int_{-\infty}^{\infty} f(x,y)e^{-i2\pi(\mu x+\nu y)}dxdy\ , \tag{10}$$

and the FT of the parallel projection $\overset{\vee}{f}_{\phi}(p)$ to the angle ϕ can be expressed in the following form:

$$\overset{\sim}{\overset{\vee}{f}}_{\phi}(w) = \int_{-\infty}^{\infty} \overset{\vee}{f}_{\phi}(p) e^{-i\pi wp} dp \,. \tag{11}$$

A simple example of the slice Fourier theorem is given by a projection in $\phi = 0$. Let us consider first that the FT of the object along a line in the frequence domain is given by $\nu = 0$. The FT described in Eq. (10) is

$$\tilde{f}(\mu,0) = \int_{-\infty}^{\infty}\int_{-\infty}^{\infty} f(x,y) e^{-i\pi\mu x} dxdy \,, \tag{12}$$

This result is due to the fact that in the phase factor, the dependence on y has been eliminated, so we can divide the integral in two parts; i. e.,

$$\tilde{f}(\mu,0) = \int_{-\infty}^{\infty}\left[\int_{-\infty}^{\infty} f(x,y)dy\right] e^{-i\pi\mu x} dx \,. \tag{13}$$

From the definition of the parallel projection, it is possible to recognize that what lies between the square brackets is an equation for the projection angle along a line with x constant. Thus, if we substitute this

$$\tilde{f}(\mu,0) = \int_{-\infty}^{\infty} \overset{\vee}{f}(x,0) e^{-i2\pi\mu x} dx \,. \tag{14}$$

In this way, the right member of the equation represents the one-dimensional FT of the projection when $\phi = 0$, since in this case, $p = x$ and $w = \mu$, Therefore, in this way we have found a relationship between the vertical projection and the 2-D transform of the object function in the following manner

$$\tilde{f}(\mu,0) = \overset{\sim}{\overset{\vee}{f}}(\mu,0) \,. \tag{15}$$

Up to this moment, it has only been proven for a particular and simple example of the Fourier slice. Nevertheless, it can be stated that this result is independent of the orientation that exists between the object and the coordinate system.

In order to deduce the Fourier slice theorem, let us consider the following rectangular coordinate axes system $(p, p_{\perp})$ and $(w, w_{\perp})$ obtained through the rotation of the axes (x, y) and (μ, ν) by an angle ϕ (as shown in Fig. 3).

$$\begin{pmatrix} p \\ p_{\perp} \end{pmatrix} = \begin{pmatrix} \cos\phi & \sin\phi \\ -\sin\phi & \cos\phi \end{pmatrix} \begin{pmatrix} x \\ y \end{pmatrix}; \quad \begin{pmatrix} w \\ w_{\perp} \end{pmatrix} = \begin{pmatrix} \cos\phi & \sin\phi \\ -\sin\phi & \cos\phi \end{pmatrix} \begin{pmatrix} \mu \\ \mu \end{pmatrix}. \tag{16}$$

It is possible to mathematically describe a sampling of the transform along a line that passes through the origin, with a slope given by ϕ :

$$\tilde{f}(\mu,\nu)\delta(-\mu\sin\phi + \nu\cos\phi) = \tilde{f}(\mu,\nu)\delta(w_{\perp}) \,, \tag{17}$$

this equation describes a mapping in the frequence Fourier space, as shown in the right-handed side of the diagram in Fig. 3, where $\delta(w_\perp)$ denotes the sampling of the transform along the line $w_\perp = 0$; i. e., along the axis w. The sampling that is obtained corresponds to the object plane with a convolution between the inverse transforms of each factor. If we now consider the fact that $\Im^{-1}\{\delta(w_\perp)\} = \delta(p)$, then for every value of ϕ, it is possible to obtain the following identities:

$$\Im^{-1}\left\{\tilde{f}(\mu,\nu)\delta(w_\perp)\right\} = \Im^{-1}\left\{\tilde{f}(\mu,\nu)\right\} \otimes\otimes \Im^{-1}\left\{\tilde{f}\,\delta(w_\perp)\right\} = f(x,y)\otimes\otimes\delta(p) = \check{f}_\phi(p), \quad (18)$$

where $\otimes\otimes$ indicates the convolution operation in two dimensions, one with respect to x and the other one with respect to y. Eq. (18) is known as the slice Fourier theorem, or the projection theorem [Haykin, 1985], and it can be stated as establishing the fact that the one-dimensional Fourier transform of the projection to the angle ϕ is identical to the sampling along a line which has a slope with an angle ϕ of the bidimensional Fourier transform of the slice function. In this proof, it has been assumed that $f(x,y)\otimes\otimes\delta(p) = \check{f}_\phi(p)$, and in order to verify this, it is possible to rewrite Eq. (7) changing the integration variables (x,y) by (ξ,η) and substituting $p = x\cos\phi + y\sin\phi$, so

$$\begin{aligned}\check{f}_\phi(p) &= \int_{-\infty}^{\infty}\int_{-\infty}^{\infty} f(\xi,y)\delta(x\cos\phi + y\sin\phi - \xi\cos\phi - \eta\sin\phi)d\xi d\eta \\ &= \int_{-\infty}^{\infty}\int_{-\infty}^{\infty} f(\xi,y)\delta\left[(x-\xi)\cos\phi + (y-\eta)\sin\phi\right]d\xi d\eta\end{aligned}, \quad (19)$$

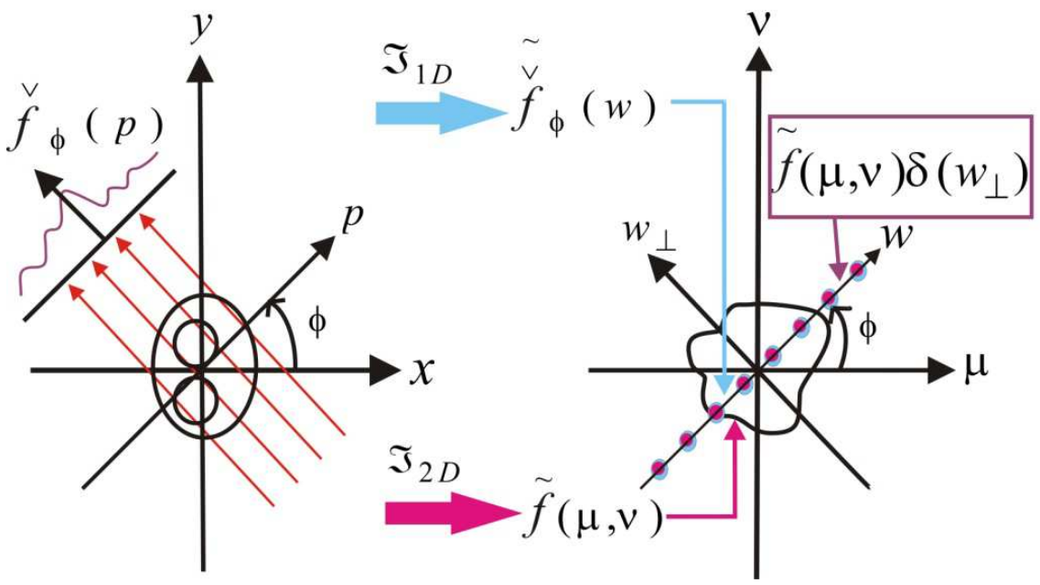

Fig. 3. Coordinate system for parallel projections. From the plane of the slice of object *f*, to the Fourier plane $\tilde{f}$.

this can be seen as a convolution of the form $f(x,y)\otimes\otimes\delta(x\cos\phi+y\sin\phi)$, which proves the last statement, since $\delta(x\cos\phi+y\sin\phi)=\delta(p)$. It can be concluded that the Radon transform can be symbolically written as a convolution of the slice function $f(x,y)$ with a Dirac delta function

$$\overset{\vee}{f}(p,\phi)=\Re\{f(x,y)\}=f(x,y)\otimes\otimes\delta(p), \tag{20}$$

hence, the slice Fourier theorem, expressed in Eq. (18), can finally be written as

$$\tilde{f}(\mu,\nu)\delta(w_{\perp})=\Im\left\{\overset{\vee}{f}_{\phi}(p)\right\}=\overset{\sim}{\overset{\vee}{f}}_{\phi}(w). \tag{21}$$

It is important to note that the convolution of the two functions in order to find the FT of Eq. (20) is identical to Eq. (21), which is the projection theorem. Therefore, the same properties of symmetry and the zero-moment of the RT must satisfied in the frequency space.

3.3 Inverse Radon transform

The inverse Radon transform can be solved interpreting the parallel projection $\overset{\vee}{f}_{\phi}(p)$ as an unidimensional inverse transform $\Im_{1D}^{-1}\{...\}$ of a sampling of the bidimensional transform $\tilde{f}=\Im_{2D}\{f(x,y)\}$ made along the line $w_{\perp}=0$. Thus, if $\overset{\vee}{f}_{\phi}(p)$ is known, then for every ϕ it is possible to state that

$$f(x,y)=\Im_{2D}^{-1}\left\{\tilde{f}(\mu,\nu)\right\}=\Im_{2D}^{-1}\left\{B\Im_{1D}\left[\overset{\vee}{f}_{\phi}(p)\right]\right\}, \tag{22}$$

where it is implied that $\tilde{f}(\mu,\nu)$ is constructed with all $\overset{\vee}{f}_{\phi}(p)$ conventionally accomodated. Here $\Im_{1D}\{...\}$, is from $p\rightarrow w$ and the accomodation is denoted by B [Deans, 1983].
If we start from the definition of the inverse Fourier transform of the slice function,

$$f(x,y)=\int_{-\infty}^{\infty}\int_{-\infty}^{\infty}d\mu d\nu\tilde{f}(\mu,\nu)e^{i2\pi(\mu x+\nu y)}, \tag{23}$$

changing to polar coordinates: $\mu=w'\cos\phi$ and $\nu=w'\sin\phi$, with $w'^2=\mu^2+\nu^2$, then $d\mu d\nu=w'dw'd\phi$, and by substituting this in the equation of the inverse bidimensional transform, the following expression is obtained:

$$f(x,y)=\int_{0}^{2\pi}d\phi\int_{0}^{\infty}w'dw'\tilde{f}(w',\phi)e^{i2\pi w'(x\cos\phi+y\sin\phi)}, \tag{24}$$

where $\tilde{f}(\mu,\nu)=\tilde{f}(w',\phi)$ and this last equation can be rewritten as:

$$f(x,y)=\int_0^{\pi}d\phi\int_0^{\infty}w'dw'\tilde{f}(w',\phi)e^{i2\pi w'(x\cos\phi+y\sin\phi)}+\int_{\pi}^{2\pi}d\phi\int_0^{\infty}w'dw'\tilde{f}(w',\phi)e^{i2\pi w'(x\cos\phi+y\sin\phi)}\,, \quad (25)$$

But if $\varphi=\varphi+\pi$ is substituted in the second term of the right-hand side of the equation,

$$f(x,y)=\int_0^{\pi}d\phi\int_0^{\infty}w'dw'\tilde{f}(w',\phi)e^{i2\pi w'(x\cos\phi+y\sin\phi)}+\int_0^{\pi}d\phi\int_0^{\infty}w'dw'\tilde{f}(w',\phi+\pi)e^{-i2\pi w'(x\cos\phi+y\sin\phi)}\,. \quad (26)$$

In the rotated coordinate system, the function $\tilde{f}(\mu,\nu)$ is described by $\tilde{f}(w,w_{\perp})$. Nevertheless, considering in particular one projection angle ϕ, it is possible to establish the fact that

$$\tilde{f}(w',\phi)=\tilde{f}(w,w_{\perp})\delta(w_{\perp})u(w)\,, \quad (27)$$

where $u(w)$ is the unitary step function or the *Heaviside* function defined under the Direclet criterion [Hwei, 1970], which selects only the positive part of the sampling of $\tilde{f}(w,w_{\perp})$ over the line $w_{\perp}=0$ along w, which is caused by $\delta(w_{\perp})$. Substituting $\tilde{f}(w,w_{\perp})=\tilde{f}(\mu,\nu)$ and applying the Fourier slice theorem,

$$\tilde{f}(w',\phi)=\tilde{\check{f}}_{\phi}(w)u(w)\,, \quad (28)$$

Selecting one half of the projection for a positive w, it is possible to prove in a similar manner that

$$\tilde{f}(w',\phi+\pi)=\tilde{\check{f}}_{\phi}(w)u(-w)\,, \quad (29)$$

which selects the other half of the projection for negative w. Making the change of variable $w'=wu(w)$, then $dw'=dwu(w)$ so substituting this in Eq. (28), in the integral of the first term of Eq. (26), and if another change of variable $w'=-wu(-w)$ is done, then $dw'=-dwu(-w)$, so by substituting Eq. (29) in the second term of Eq. (26), it is possible to arrive to the conclusion that

$$f(x,y)=\int_0^{\pi}d\phi\int_{-\infty}^{\infty}wu(w)dw\tilde{\check{f}}_{\phi}(w)e^{i2\pi wp}-\int_0^{\pi}d\phi\int_{-\infty}^{\infty}wu(-w)dw\tilde{\check{f}}_{\phi}(w)e^{i2\pi wp}\,, \quad (30)$$

where it has been assumed that $\exp\left[i2\pi wu(\pm w)p\right]=u(\mp w)+u(\pm w)\exp(i2\pi wp)$, where $u^n(\pm w)=u(\pm w)$ with n real, and $u(w)u(-w)=0$. By grouping the integrals, we have

$$f(x,y)=\int_0^{\pi}d\phi\int_{-\infty}^{\infty}w\left[u(w)-u(-w)\right]dw\tilde{\check{f}}_{\phi}(w)e^{i2\pi wp}\,, \quad (31)$$

and by rewriting the *signum* function in terms of the *Heaviside* function in the form $\mathrm{sgn}(w) = u(w) - u(-w)$ [Ronald, 2000]; it is possible to conclude that $|w| = w\left[u(w) - u(-w)\right]$, where the bars indicate an absolute value, so we finally arrive to the following expression

$$f(x,y) = \int_0^{\pi} d\phi \int_{-\infty}^{\infty} |w|\, dw\, \tilde{\check{f}}_{\phi}(w) e^{i2\pi wp} , \tag{32}$$

If the filtered projection is defined with a spatial filter of the form $\check{g}_{\phi}(p) = \int_{-\infty}^{\infty} dw |w| \tilde{\check{f}}_{\phi}(w) e^{i2\pi wp}$, then

$$\check{g}_{\phi}(p) = \Im^{-1}\left\{ |w| \tilde{\check{f}}_{\phi}(w) \right\} = \int_{-\infty}^{\infty} dw |w| \tilde{\check{f}}_{\phi}(w) e^{i2\pi wp} , \tag{33}$$

so the inverse Radon transform can be written as

$$f(x,y) = \int_0^{\pi} d\varphi\, \check{g}_{\phi}(p) = \int_0^{\pi} d\phi\, \check{g}_{\phi}(x\cos\phi + y\sin\phi) . \tag{34}$$

This result establishes the existence of a possible inverse Radon transform operation which is mediated by a spatial filter $|w|$. This is the reason why it is known as a filtered projection, and Eq. (34) is known as the retroprojection of the filtered projections. It is important to note that the resulting filter is reminiscent of the derivative (by a linear factor w) [Deans, 1983].

4. Numerical simulation

A numerical simulation is a mathematical recreation of a natural process. By using numerical simulations, it is possible to study physical processes. Thus, the field of numerical simulations represents a rich field of interdisciplinary research. Some of the scientific problems are studied principally through the use of numerical simulations, such as those scientific fields that are governed by non-linear simultaneous equations, or those that are not easily reproducible in the laboratory. The use of these to study a problem normally requires a careful study of the numerical methods and algorithms that will be used and the fundamental process that will be included. A numerical simulation differs from a mathematical model in the sense that the first one is a representation in every instant of the process that will be simulated, while the second one is a mathematical abstr5action of the fundamental equations necessary to analyze the phenomenon. Normally, the use of a numerical simulation in the analysis of a given problem requires a careful planning of the mathematical model that will be used and the necessary algorithms that will be employed.

The numerical simulation presented here will have the following steps:

1. Definition of the slice function of the object $f(x,y)$,
2. Calculation of the profiles or parallel projections of the object $\check{f}_{\phi}(p)$ for every ϕ in the range $[0,2\pi]$, and

3. Calculation of the reconstruction of the slice of the object through the filtered retroprojection algorithm.

Fig. 4(a) presents a slice of an object in a finite domain in gray levels and in 3D, where in the sake of simplicity, a unitary value has been assigned inside, and it is null outside this domain. The image shown has a resolution of 200x200 pixels and is encoded in 256 gray levels. The slice of the object generally is a cross section at a constant height of the study object. Once the slice function $f(x,y)$ has been defined, it is necessary to calculate the projections through the implementation of the Radon transform. This sample is identified with a sinogram, as can be seen in Fig. 4(b) in 2D and 3D. A sinogram is a data matrix, where the number of rows represents the number of projections taken between 0 and 2π radians; i. e. ϕ, and the number of columns is the number of samples considered in the projection coordinates p. Each row is identified with a projection angle and the data in these can be seen as a profile in this angle. The angular step $\Delta\phi = \pi/100$ was used, where 200 was the number of projections calculated, while the number of data for each projection was of 200, so the sinogram has a resolution of 200 x 200 pixels, and it is encoded in 256 levels of grays.

Respect to the reconstruction of the slice of the object, in this chapter, the filtered retroprojection algorithm is used [Deans, 1983], which is a discrete implementation of the inverse Radon transform. The filtered retroprojection algorithm was first proposed by Bracewell and Riddle [Bracewell & Riddle, 1967] and was also stated independently by Ramachandran and Lakshminarayanan [Ramachandran & Lakshminarayanan, 1971]. The superiority of the filtered retroprojection algorithm when compared to the algebraic techniques was first proven by Shepp and Logan [Shepp & Logan, 1974]. This was developed for data with a form of a fan, and it was done by Lakshminarayanan [Lakshmnarayanan, 1975] for the case of equidistant collinear detectors, and was later extended by Herman and Naparstek [Herman & Naparstek, 1977] for the case of equiangular rays. Several authors [Baba & Murata, 1977] [Kenue & Greenleaf, 1979] [Kwoh *et al*., 1977] [Lewitt, 1979] [Tanaka & Iinuma, 1975] have proposed variations to the filter function of the filtered retroprojection algorithm. The images can be reconstructed from data from beams that have a fan form. The filtered retroprojection algorithm was used for reconstructions that were done from data generated by the use of very narrow angles in a fan form and beams that rotate and cross continuously the surroundings of the object. The projection algorithm is also known for non-uniform data of the sample [Horn, 1978] [Horn, 1979] [Lewitt & Bates, 1978] [Oppenheim, 1975] [Sato *et al.,* 1980] [Tam & Perez-Mendez, 1981] and for reconstructions obtained from incomplete and limited projections.

Complete reconstructions in three dimensions are discussed in [Chiu *et al*., 1979] [Chiu *et al*., 1980] [Smith, 1985]. It is also possible to obtain tomographic images with the use of the direct inverse Fourier transform, although it has less precision, instead of using the filtered retroprojection method. This was proven first by Bracewell [Bracewell, 1956] in radio astronomy, and afterwards it was also done independently by DeRosier and Bracewell [DeRosier & Klug, 1968] for electronic microscopy and Rowley [Rowley, 1969] in optic holography. Several authors apply this method to the radiography, such as Tretiak [Tretiak *et al*., 1969]. In order to use 2-D FFT algorithms for image formation, they focus specially on the direct Fourier approximation. For some methods that are more recent that reduce to the minimum the resultant interpolation error, you can see [Stark *et al*., 1981]. Recently, Wernecke and D'Addario [Wernecke & D'Addario, 1977] have proposed an approach of

maximum entropy to direct the Fourier inverse. Their procedure is especially useful if for some reason, the projection of the data is insufficient. A more extensive discussion about these algorithms, as well as the study of their characteristic artifacts is beyond the present study.

The implementation of the filtered retroprojection, in the first place, requires the calculation of the filtered projection (Eq. 34), which is implemented in an approximated manner, introducing a limited bandwidth,

$$g_\phi(p) = \int_{-\Gamma}^{\Gamma} dw|w| \tilde{\check{f}}_\phi(w) e^{i2\pi wp} \ . \tag{35}$$

The projection with a bandwidth Γ must satisfy the Nyquits criterion, $\Gamma = 1/2\varepsilon$ where ε is the sampling range of the projection. Under this condition, the original ramp function $|w|$ is multiplied by a window function $rect(w/2\Gamma)$, $H(w) = |w| rect(w/2\Gamma)$. Another type of window, such as the Hanning, hamming, etc, have also been used [Deans, 1983], so under these considerations, it is possible to describe the impulse response that validates a data sample [Deans, 1983]

$$h(n\varepsilon) = \begin{cases} \frac{1}{4\varepsilon^2} & n = 0 \\ 0 & n = par \\ -\frac{1}{n\pi\varepsilon^2} & n = impar \end{cases} \tag{36}$$

If the discrete number of the projection is denoted by $\check{f}_\phi(k\varepsilon)$ $(k = 0,...N-1)$ at the angle ϕ, the filtered projection described by Eq. (34) can be expressed as a convolution in the spatial domain as

$$g_\phi(n\varepsilon) = \varepsilon \sum_{k=0}^{N-1} h([n-k]\varepsilon) \check{f}_\phi(\mathrm{k}\varepsilon), \quad n = 0,1,...,N-1. \tag{37}$$

Continuing with the procedure in order to obtain the object reconstruction, the filtered projection is adequately introduced in the retroprojection sum

$$b(x,y) = \sum_{m=0}^{M-1} g_\phi\left(x\cos\left(m\Delta\phi\right) + y\sin\left(m\Delta\phi\right)\right), \tag{38}$$

this comes from the suggesting integral of the inverse Radon transform of *f*, Eq. (34), where ϕ increases by steps $\Delta\phi$, and for some point $p = n\varepsilon$ and ϕ=m$\Delta\phi$ the transformation points (x,y) must satisfy $n\varepsilon = x\cos(m\Delta\phi) + y\sin(m\Delta\phi)$. If we choose $\varepsilon = 1$, in the simulation and applying successively Eqs. (36-38), the sinogram obtained in Fig. 4-(b), the reconstruction of the defined object in Eq. (22) is obtained, as shown in Fig. 4(c) [Deans, 1983].

5. Tomography of enhanced edges using the Hilbert transform

As was mentioned before, the internal information of the object under study can be retrieved from the projections measured with adequate inversion techniques with having to

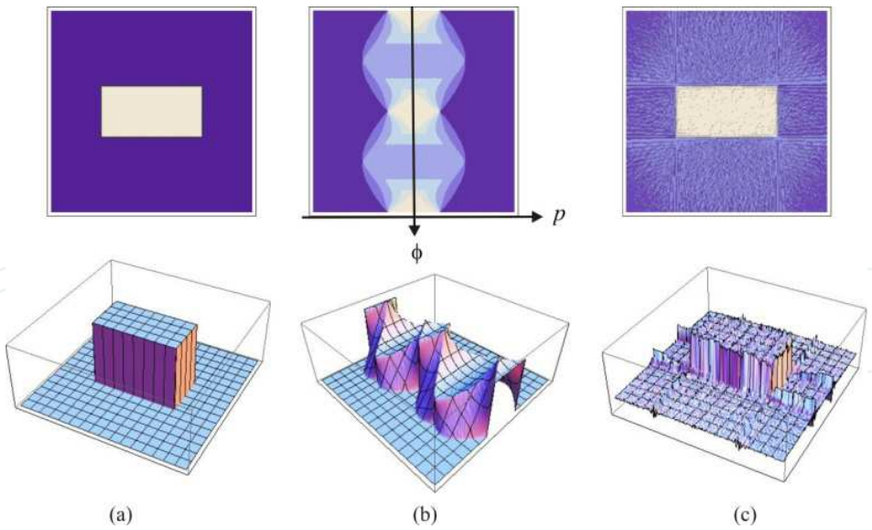

Fig. 4. (a) Slice of the object $f(x,y)$ in 2-D and 3-D; (b) sinogram corresponding to the slice of the object in 2-D and 3-D; (c) reconstruction of the slice of the object in 2-D and 3-D.

cut or damage the sample. In this section, a mathematical model is shown to retrieve the Hilbert transform of the slice function instead of only the slice function. It will be proven that this transform can be obtained in a directional manner in 2-D, and this effect can be accomplished in a spatial filtering process in the frequency domain of the projection. It will be shown that this idea, applied to optical tomography of phase objects can find, for the case of thin phase objects, the directional Hilbert transform of the refraction index distribution, which results in a directional edge enhancement of the reconstructed image, and in the case of thick phase objects, it will be shown that an isotropic edge enhancement of the refraction index can be found. This is based on the relationship that the Hilbert transform has with the Radon transform, as will be stated below.

5.1 The Hilbert transform

It is known that the Hilbert transform is a useful mathematical tool for the description of the complex envelope of the modulated signal for a real carrier. Mathematically, in one dimension, the transform is defined in the following manner [Abhilash, 2006]

$$\overset{\frown}{s}(x) = H\{s(x)\} = \frac{1}{\pi}\int_{-\infty}^{\infty}\frac{s(x')}{x-x'}dx' = \frac{1}{\pi x}\otimes s(x)\,, \tag{39}$$

where $s(x)$ is the input function, $\overset{\frown}{s}(x)$ is its corresponding Hilbert transform, and $H\{\cdots\}$ is the respective operator. The integral is evaluated in its principal value. The last term indicates that the Hilbert transform can be written in a symbolic manner as the convolution of the input signal with the function $1/\pi x$.

The typical procedure commonly used for the calculation of the Hilbert transform of a function is done using Fourier analysis [Poularikas, 2000]

$$\overset{\frown}{s}(x) = H\{s(x)\} = \Im^{-1}\left\{-i\,\mathrm{sgn}(\mu)\tilde{s}(\mu)\right\}, \tag{40}$$

where the convolution property of the Fourier transform has been applied, with $s(\mu)=\Im\{s(x)\}$ and $-i\,\mathrm{sgn}(\mu)=\Im\{1/\pi x\}$ [Abhilash, 2006], where $\mathrm{sgn}(\mu)$ is known as the *signum* function, which is a special function defined as

$$-i\,\mathrm{sgn}(\mu)=\begin{cases}-i, & \mu>0\\ 0, & \mu=0\\ -i, & \mu<0\end{cases}, \tag{41}$$

in general, the *signum* function is undefined at $\mu=0$, but here, it has been defined as equal to zero under the Direchlet criterion [Seeley, 1970].

The expression enclosed between brackets in Eq. (40) can be interpreted as a filter operation in a linear system, with $-i\,\mathrm{sgn}(\mu)$ having the role of the filter in the spectral domain of the signal $s(x)$, and its corresponding Fourier inverse $1/\pi x=\Im^{-1}\{-i\,\mathrm{sgn}(\mu)\}$ as a consequence of the input. The operation can be seen as a phase change of $+\pi/2$ radians for each one of the positive frequency components of the signal and a phase change of $-\pi/2$ radians for each one of the negative frequency components of the signal, without changing its amplitude. For this reason, an experimental implementation is viable in areas in which the signal treatment is possible; for example, in communication systems with electric signals [Almeida, 1994] or in optical data processing in Fourier optics [Philipp *et al*., 1992].

In two dimensions, the HT has been defined in several ways, being one of the most used [Abhilash, 2006]

$$\overset{\frown}{s}(x,y)=H\{s(x,y)\}=\frac{1}{\pi^2}\int_{-\infty}^{\infty}\int_{-\infty}^{\infty}\frac{s(x',y')}{(x-x')(y-y')}dx'dy'=\frac{1}{\pi^2 xy}\otimes\otimes s(x,y), \tag{42}$$

Again, the integrals are evaluated in their respective principal Cauchy value. One definition in n dimensions can be seen in [Poularikas, 2000]. On the other hand, the partial Hilbert transforms have also been defined [Poularikas, 2000]. For example, the partial transform with respect to x has the form

$$\overset{\frown}{s}^{0}(x,y)=H^0\{s(x,y)\}=\frac{1}{\pi}\int_{-\infty}^{\infty}\frac{s(x',y)}{x-x'}dx', \tag{43}$$

and with respect to y, it has the form

$$\overset{\frown}{s}^{\frac{\pi}{2}}(x,y)=H^{\frac{\pi}{2}}\{s(x,y)\}=\frac{1}{\pi}\int_{-\infty}^{\infty}\frac{s(x,y')}{y-y'}dy', \tag{44}$$

where the superindices are angles in radians, that indicate the direction in which the transform operation is done, although for the x direction, the notation $\overset{\frown}{s}_x(x,y)$ is more commonly used, and for the y direction, $\overset{\frown}{s}_y(x,y)$ is more extensively employed. In these expressions, the angles 0 and $\pi/2$ have been used as superscripts. This notation has been selected for simplicity, and in order to avoid a possible ambiguity with the notation used in tomography. In a symbolical form, for x this can be written as

$$\overset{\cap}{s}^{0}(x,y)=\frac{\delta(\mathrm{y})}{\pi x}\otimes\otimes s(x,y)\,, \tag{45}$$

and for the variable y

$$\overset{\cap}{s}^{\frac{\pi}{2}}(x,y)=\frac{\delta(x)}{\pi y}\otimes\otimes s(x,y)\,. \tag{46}$$

In a similar manner, we define the directional Hilbert transform in the form

$$\overset{\cap}{s}^{\alpha}(x,y)=H^{\alpha}\{s(x,y)\}=\frac{1}{\pi}\int_{-\infty}^{\infty}\int_{-\infty}^{\infty}\frac{\delta\left[-(x-x')\sin\alpha+(y-y')\cos\alpha\right]}{(x-x')\cos\alpha+(y-y')\sin\alpha}s(x',y')dx'dy'\,, \tag{47}$$

and in a symbolic form,

$$\overset{\cap}{s}^{\alpha}(x,y)=\frac{\delta(-x\sin\alpha+y\cos\alpha)}{\pi(x\cos\alpha+y\sin\alpha)}\otimes\otimes s(x,y)\,, \tag{48}$$

where the angle α is expressed in radians, and it denotes the direction at which the Hilbert transform is done. It is important to note that the partial Hilbert transform with respect to x and y as defined in Eqs. (45) and (46) can be derived from the definition of the directional Hilbert transform when $\alpha=0$ and when $\alpha=\pi/2$, respectively.
Using Fourier analysis, the directional transform can be defined using the convolution property in two dimensions through

$$\overset{\cap}{s}^{\alpha}(x,y)=\Im^{-1}\left\{-i\,\mathrm{sgn}(\mu\cos\alpha+\nu\sin\alpha)\tilde{s}(\mu,\nu)\right\}, \tag{49}$$

where $\tilde{s}(\mu,\nu)=\Im\{s(x,y)\}$ and
$-i\,\mathrm{sgn}(\mu\cos\alpha+\nu\sin\alpha)=\Im\{\delta(-x\sin\alpha+y\cos\alpha)/\pi(x\cos\alpha+y\sin\alpha)\}$, which can be proved in the following manner. Using the integral definition of the Fourier transform,

$$\Im\left\{\frac{\delta(-x\sin\alpha+y\cos\alpha)}{\pi(x\cos\alpha+y\sin\alpha)}\right\}=\int_{-\infty}^{\infty}\int_{-\infty}^{\infty}\frac{\delta(-x\sin\alpha+y\cos\alpha)}{\pi(x\cos\alpha+y\sin\alpha)}\exp\left[-i2\pi(\mu x+\nu y)\right]dxdy\,, \tag{50}$$

rotating by an angle α both coordinate systems (x,y) and (μ,ν), it is possible to state that

$$\begin{pmatrix}x\\y\end{pmatrix}=\begin{pmatrix}r\cos\alpha-r_{\perp}\sin\alpha\\r\sin\alpha+r_{\perp}\cos\alpha\end{pmatrix}\ \text{and}\ \begin{pmatrix}\mu\\\nu\end{pmatrix}=\begin{pmatrix}\sigma\cos\alpha-\sigma_{\perp}\sin\alpha\\\sigma\sin\alpha+\sigma_{\perp}\cos\alpha\end{pmatrix}, \tag{51}$$

where the rotated coordinates have been denoted by $(r,r_{\perp})$ and $(\sigma,\sigma_{\perp})$, respectively and thus, $dxdy=drdr_{\perp}$, $\mu x=\sigma r$, and $\nu y=\sigma_{\perp}r_{\perp}$. Substituting Eq. (51) in Eq. (50),

$$\Im\left\{\frac{\delta(-x\sin\alpha+y\cos\alpha)}{\pi(x\cos\alpha+y\sin\alpha)}\right\}=\int_{-\infty}^{\infty}\int_{-\infty}^{\infty}\frac{\delta(r_{\perp})}{\pi r}\exp\left[-i2\pi(\sigma r+\sigma_{\perp}r_{\perp})\right]drdr_{\perp}\,. \tag{52}$$

This equation can be written as a separable integral

$$\Im\left\{\frac{\delta(-x\sin\alpha+y\cos\alpha)}{\pi(x\cos\alpha+y\sin\alpha)}\right\}=\int_{-\infty}^{\infty}\frac{1}{\pi r}\exp(-i2\pi\sigma r)dr\int_{-\infty}^{\infty}\delta(r_{\perp})\exp(-i2\pi\sigma_{\perp}r_{\perp})dr_{\perp}\,, \tag{53}$$

where each factor is a one-dimensional Fourier transform that is known, the first being $\Im\{1/\pi r\}=-i\,\mathrm{sgn}(\sigma)$ and the second one is $\Im\{\delta(r_{\perp})\}=1$, so the solution is given by

$$\Im\left\{\frac{\delta(-x\sin\alpha+y\cos\alpha)}{\pi(x\cos\alpha+y\sin\alpha)}\right\}=-i\,\mathrm{sgn}(\sigma)\,, \tag{54}$$

Finally, by direct substitution of $\sigma=\mu\cos\alpha+\nu\sin\alpha$ the following expression is obtained:

$$\Im\left\{\frac{\delta(-x\sin\alpha+y\cos\alpha)}{\pi(x\cos\alpha+y\sin\alpha)}\right\}=-i\,\mathrm{sgn}(\mu\cos\alpha+\nu\sin\alpha)\,, \tag{55}$$

which proves the point. It is thus important to note that the corresponding expressions for the definitions of the partial Hilbert transform can be directly obtained from Eq. (49) using Fourier analysis by substituting $\alpha=0$ for the partial derivative with respect to *x*:

$$\overset{\cap}{s}^{0}(x,y)=\Im^{-1}\left\{-i\,\mathrm{sgn}(\mu)\tilde{s}(\mu,\nu)\right\}, \tag{56}$$

and $\alpha=\pi/2$ for the partial with respect to *y*:

$$\overset{\cap}{s}^{\frac{\pi}{2}}(x,y)=\Im^{-1}\left\{-i\,\mathrm{sgn}(\nu)\tilde{s}(\mu,\nu)\right\}, \tag{57}$$

The definition of the directional Hilbert transform and the slice theorem will serve as a basis to establish the relationship that the Hilbert transform has with the Radon transform, and afterwards to establish how the directional Hilbert transform can be obtained of the slice function of the object study [Meneses-Fabian *et. al.,* 2011].

5.2 Tomography and the Hilbert transform

Starting from the projection data $\overset{\vee}{f}_{\phi}(p)$, in the first place it is necessary to calculate the Hilbert transform for every projection angle, to prove that this new projection data is still valid from the point of view of tomography. Then the proofs of symmetry and zero-momentum of the Radon transform, and it is proven that the partial Hilbert transform of the slice of the object with respect to *y* is reconstructed. In the second place, after finding the directional Hilbert transform of the slice function $f(x,y)$, we proceed to establish the filter function in the frequency space of the projection in order to reconstruct the directional Hilbert transform of $f(x,y)$ as if we had begun from the projection data $\overset{\vee}{f}_{\phi}(p)$.

The Hilbert transform of the projection $\overset{\vee}{f}_{\phi}(p)$ using the definition given in Eq. (49) is

$$\overset{\frown}{\underset{\vee}{f}}_{\phi}(p) = H\{\overset{\vee}{f}_{\phi}(p)\} = \overset{\vee}{f}_{\phi}(p) \otimes \frac{1}{\pi p}. \tag{58}$$

In order to prove the symmetry property, it is necessary to substitute $\phi = \phi + \pi$ and we proceed in an analogous manner to the one followed in section (3.1),

$$\begin{aligned} \overset{\frown}{\underset{\vee}{f}}_{\phi+\pi}(p) &= \overset{\vee}{f}_{\phi+\pi}(p) \otimes \frac{1}{\pi p} \\ &= -\overset{\vee}{f}_{\phi}(-p) \otimes \frac{1}{\pi(-p)}, \\ &= -\overset{\frown}{\underset{\vee}{f}}_{\phi}(-p) \end{aligned} \tag{59}$$

the negative sign that is outside the function reveals that the property is not satisfied. One half of the projections is multiplied by +1 and the other one by -1. In order to compensate this, it has been observed that the function $\mathrm{sgn}[\sin(\phi)]$ can successfully compensate the negative sign, because $\sin(\phi)$ is positive when $\phi \in (0,\pi)$, and it is negative when $\phi \in (\pi, 2\pi)$. In this manner, the new projection is given by

$$\mathrm{sgn}[\sin\phi]\overset{\frown}{\underset{\vee}{f}}_{\phi}(p) = \mathrm{sgn}[\sin\phi]\overset{\vee}{f}_{\phi}(p) \otimes \frac{1}{\pi p}. \tag{60}$$

This projection satisfies the symmetry property. In order to prove the zero momentum of the RT,

$$\begin{aligned} \int_{-\infty}^{\infty} dp\,\mathrm{sgn}[\sin\phi]\overset{\frown}{\underset{\vee}{f}}_{\phi}(p) &= \int_{-\infty}^{\infty} dp\,\mathrm{sgn}[\sin\phi]\overset{\vee}{f}_{\phi}(p) \otimes \frac{1}{\pi p} \\ &= \mathrm{sgn}[\sin\phi] \int_{-\infty}^{\infty} \mathrm{d}p \int_{-\infty}^{\infty} \mathrm{d}q\, \overset{\vee}{f}_{\phi}(q) \frac{1}{\pi(p-q)} \quad , \\ &= \mathrm{sgn}[\sin\phi] \int_{-\infty}^{\infty} \mathrm{d}q\, \overset{\vee}{f}_{\phi}(q) \frac{1}{\pi} \int_{-\infty}^{\infty} \frac{dp}{(q-p)} = 0 \end{aligned} \tag{61}$$

where it has been assumed that $\frac{1}{\pi}\int_{-\infty}^{\infty} \frac{dp}{(q-p)}$ is the Hilbert transform of the unity, which is equal to zero, $H\{1\} = 0$. In this manner, it is proven that it is a constant equal to zero and independent respect to the projection angle, so the zero-momentum property of the RT is also satisfied. In this moment, it is possible to state that a set of modified projection data, as those indicated in Eq. (60) is considered enough to reconstruct the slice function. Up to this moment, it is not possible to analytically describe this function. In order to deduce it, the modified projection indicated in Eq. (60) can be expressed using Fourier analysis:

$$\mathrm{sgn}(\sin\phi)\overset{\frown}{\underset{\vee}{f}}_{\phi}(p) = \mathrm{sgn}(\sin\phi)\,\Im^{-1}\left\{-i\,\mathrm{sgn}(w)\,\tilde{\overset{\vee}{f}}_{\phi}(w)\right\}, \tag{62}$$

Applying the slice Fourier theorem and rearranging the terms,

$$\operatorname{sgn}(\sin\phi)\overset{\diamond}{f}_{\phi}(p)=\Im^{-1}\left\{-i\operatorname{sgn}(w\sin\phi)\tilde{f}(\mu,\nu)\delta(w_{\perp})\right\}, \tag{63}$$

Using Eq. (16), and taking into account the filter property of the delta function, it is possible to find that $\operatorname{sgn}(w\sin\phi)=\operatorname{sgn}(v)$, and obtaining the inverse Fourier assuming that the convolution property for the triple product is given by the convolution of each one of the individual inverses, it can be proven that

$$\operatorname{sgn}(\sin\phi)\overset{\diamond}{f}_{\phi}(p)=\left[\frac{\delta(x)}{\pi y}\otimes\otimes f(x,y)\right]\otimes\otimes\delta(p)=\overset{\frown}{f}^{\frac{\pi}{2}}(x,y)\otimes\otimes\delta(p)=\overset{\vee}{\overset{\frown}{f}}{}^{\frac{\pi}{2}}_{\phi}(p), \tag{64}$$

where it has been assumed that what is enclosed between brackets is the definition of the partial Hilbert transform respect to y, and in this manner, the following relationship can be stated,

$$\operatorname{sgn}(\sin\phi)H\left\{\Re_{\phi}\left\{f(x,y)\right\}\right\}=\Re_{\phi}\left\{H^{\frac{\pi}{2}}\left\{f(x,y)\right\}\right\}, \tag{65}$$

which means that the Hilbert transform of a projection at an angle ϕ mediated by a sign factor from the sine of the projection angle equal to the projection of the partial Hilbert transform with respect to y of the slice function. This result predicts that the partial Hilbert transform respect to y will be reconstructed when each parallel projection will be calculated. Their Hilbert transform will have as a result an edge enhancement in the vertical direction.

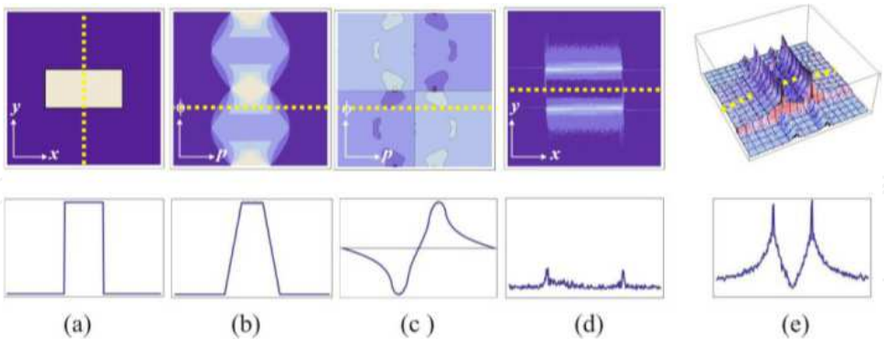

Fig. 5. Numerical simulation. Edge-enhancement along the vertical direction of a unitary rectangle used as the slice function of a thin phase object: (a) slice, (b) sinogram, (c) Hilbert-sinogram, (d-e) vertical edge enhancement reconstruction. The second row shows a line or column data corresponding to each image at first row as is indicated with the yellow dotted line.

Fig. 5 shows a numerical simulation of the theory mentioned above. Column (a) shows the slice of the object $f(x,y)$, while the lower image shows the plot of the profile of the function along the dotted vertical line that crosses the rectangle in the center. Column (b) shows the

sinogram of $f(x,y)$. The image of the upper part of column (c) shows the convolution for each one of the projections in the sinogram that are consequence of the input of the system $1/\pi p$ with the corresponding sign compensation, as indicated in Eq. (60). Observe that the signs of the projections change around $\phi = \pi$, as a result of the symmetry property of the Radon transform. We have denominated this modified sinogram as a Hilbert-sinogram. The lower image shows a sketch of the Hilbert transform of the projection along the same angle used for the last profile. Moreover, with the use of a filtered retroprojection algorithm, the tomographic reconstruction is obtained. The images of the column (d-e) present the reconstruction of the slice function in 2-D and 3D, respectively, where the edge enhancement in the vertical direction is shown, as was expected. The images in the lower part show the profile of the dotted line in the reconstructed image. The line in (d) selects a row of the reconstructed image, as shown in the lower image, and the line in (e) selects one profile of the image, presenting an edge enhancement on the vertical direction.
In this point, and with the purpose of generalizing this discussion, the directional Hilbert transform is calculated using the definition (48) of the slice function.

$$\overset{\cap}{f}{}^{\alpha}(x,y)=\frac{\delta(-x\sin\alpha+y\cos\alpha)}{\pi(x\cos\alpha+y\sin\alpha)}\otimes\otimes f(x,y)\,. \tag{66}$$

The projection at an angle ϕ is symbolically given by

$$\overset{\vee}{\overset{\cap}{f}}{}^{\alpha}_{\phi}(p)=\frac{\delta(-x\sin\alpha+y\cos\alpha)}{\pi(x\cos\alpha+y\sin\alpha)}\otimes\otimes f(x,y)\otimes\otimes\delta(p)\,. \tag{67}$$

Applying the convolution property for the triple product of functions in the Fourier space, Eq. (67) will be given by

$$\overset{\sim}{\overset{\vee}{\overset{\cap}{f}}}{}^{\alpha}_{\phi}(w)=-i\,\mathrm{sgn}(\mu\cos\alpha+\nu\sin\alpha)\,\tilde{f}(\mu,\nu)\delta(w_{\perp})\,. \tag{68}$$

Rotating the coordinates using Eq. (16), it is possible to demonstrate the equation $\mu\cos\alpha+\nu\sin\alpha=w\cos(\phi-\alpha)-w_{\perp}\sin(\phi-\alpha)$, and by taking this into account, the last expression can be simplified to the following expression:

$$\overset{\sim}{\overset{\vee}{\overset{\cap}{f}}}{}^{\alpha}_{\phi}(w)=-i\,\mathrm{sgn}[w\cos(\phi-\alpha)]\,\overset{\sim}{\overset{\vee}{f}}(w)\,, \tag{69}$$

where the filter property of the Dirac delta function and the slice Fourier theorem have been applied. Calculating the inverse Fourier transform for both sides of the equation,

$$\overset{\vee}{\overset{\cap}{f}}{}^{\alpha}_{\phi}(p)=\mathrm{sgn}\left[\cos(\phi-\alpha)\right]\frac{1}{\pi p}\otimes\overset{\vee}{f}_{\phi}(p)=\mathrm{sgn}\left[\cos(\phi-\alpha)\right]\overset{\cap}{\overset{\vee}{f}}_{\phi}(p)\,, \tag{70}$$

where it has been assumed that the relationship $\operatorname{sgn}\left[w\cos\left(\phi-\alpha\right)\right]=\operatorname{sgn}\left(w\right)\operatorname{sgn}\left[\cos\left(\phi-\alpha\right)\right]$ is satisfied. Therefore, the projection of the Hilbert transform of the slice function $f\left(x,y\right)$ along the direction indicated by α is identical to a Hilbert transform of the projection at an angle ϕ mediated by a sign factor by the cosine of the projection angle and the director angle. It is important to note that when $\alpha=\pi/2$, Eq. (70) is reduced to the particular case stated in Eq. (65). Expressing the last expression in terms of operators,

$$\Re_{\phi}\left\{H^{\alpha}\left\{f\left(x,y\right)\right\}\right\}=\operatorname{sgn}\left[\cos\left(\phi-\alpha\right)\right]H\left\{\Re_{\phi}\left\{f\left(x,y\right)\right\}\right\}, \tag{71}$$

i. e., the Radon transform of the directional Hilbert transform of the slice function is identical to the Hilbert transform of the projection mediated by the *signum* function of the cosine of the projection angle and the angle that is indicated by the operation.

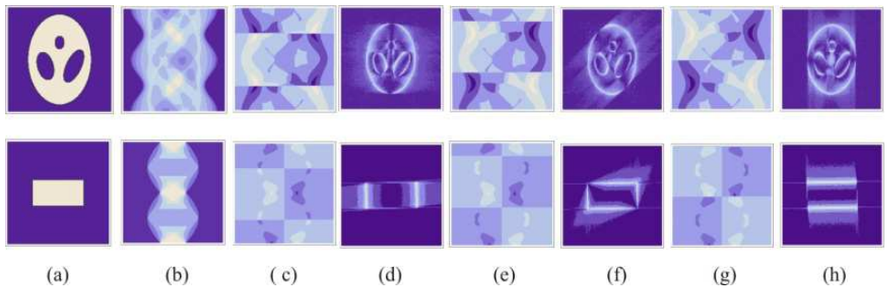

Fig. 6. Reconstruction of the directional Hilbert transform of the slice function. Two examples of slices are presented: (a) phatom of Shepp-Logan, (b) sinograms, (c, e, g) Hilbert-sinograms of irradiance with $\alpha=0,\pi/4,\pi/2$, respectively, (d, f, g); direction reconstruction of the Hilbert-sinograms of (c, e, g).

Fig. 6 presents a numerical simulation of directional edge-enhancement tomography for two slice functions and three particular directions. In column (a) slice functions, Shepp-Logan (upper image) and a rectangle (lower image) are shown. It is important to mention that the first row shows everything related with the Shepp-Logan, while the second row presents everything that is related to the rectangle. The column (b) shows the sinograms for each one of the slices indicated in (a); in the columns (d), (f), and (h), there are reconstructions of the Hilbert-sinograms shown in (c), (e), and (f). In this simulation, the reconstruction of the directional Hilbert transform of the slice function is obtained, just in the manner stated above.

5.3 Optical tomography of edge-enhancement

When the diffraction and refraction effects are significant, it becomes impossible to predict the path of a ray. If the algebraic techniques are applied under these conditions, it is very common to obtain insignificant results. If the refraction and diffraction effects are small (in inhomogeneous media, they are less than 2 for the 3% of the average value and the correlation width for these inhomogeneities is much greater that the wavelength), in some cases it is possible to combine algebraic techniques with digital ray tracing [Andersen & Kak, 1982], who designed iterative procedures that first construct the corresponding transmittance and receive the positions using this distribution, and finally use these rays to construct a more exact series of algebraic equations. Experimentally, this iterative procedure

has been verified for low refraction objects. In particular, when a light beam crosses an object and only suffers phase changes, it is considered as a phase object. In the study of these kinds of objects, in terms of optical tomography, a minimum refraction is assumed (refractional limits). In this approximation, the light rays travel in straight lines and cross the object without changing their path, so it is possible to not to take into account the changes of diffraction, dispersion, polarization, refraction, etc.

In the last section, the theory required for reconstructing the directional Hilbert transform of the slice function was stated, instead of only the slice function, which was proved with a numerical simulation and taking tomographic images with edge enhancement. In this section, we will present how this idea can be implemented in an experiment applied to optics. In particular, thin phase objects will be presented, where well described analytic relations are obtained, and an approximated description for the case of non-thin phase objects will be stated, in which there is an isotropic enhancement instead of the directional enhancement. This experimental implementation is based on obtaining the Hilbert transform in the optical field, which is done through the implementation of an optical correlator or a 4*f* image forming system of a double Fourier transform.

5.3.1 Hilbert transform using a 4*f* system

It is well known that the implementation of the Hilbert transform using an optical system can be efficiently implemented employing a double Fourier transform 4*f* image system, also known as an optical correlator. Its functioning is based on the optical Fourier theory. There are several proposals to optically implement the two-dimensional Hilbert transform. Some have proposed to obtain the transform under a rectangular system [Davis *et. al.,* 2000] with a sign filter and others say that it is possible to find the radial Hilbert transform with a spiral step filter [Davis *et. al.,* 2000]. There are also others who suggest the implementation of a fractional Hilbert transform in rectangular coordinates with a variable phase step filter [Davis *et. al.,* 2002]. It has already been proven that the Hilbert transform of the optical field shows an edge enhancement in terms of the image, and it is noteworthy to state that this fact has been used in optical image processing. In the implementation discussed here, a phase step filter of π radians will be used to obtain the partial Hilbert transform respect to the projection coordinate, and to obtain the one-dimensional Hilbert transform of the field that goes out of the object at a height z. On the other hand, it is important to mention that the implementation of the 4*f* system to obtain the partial Hilbert transform of the field will constitute the bases to construct an optical tomographer used to get tomographic images with experimental edge-enhancement.

5.3.1.1 Statement of the problem

In order to begin the discussion, let us assume that there is a homogeneous plane wave without slope and with amplitude A, linearly polarized, which propagates in the positive direction of $p_{\perp}$, whose spatial part is described by $t_A(p,z)=A$. If this wave crosses the phase object described in a right-handed coordinate system, whose refraction index is a point of the sample denoted by $f(x,y,z)$, then the wave that exits the object is given by

$$A_{\phi}(p,z)=A\exp\left[i\frac{2\pi}{\lambda}\overset{\vee}{f}_{\phi}(p,z)\right], \tag{72}$$

where λ is the wavelength of the light used and $\overset{\vee}{f}_{\phi}(p,z)$ is the accumulated optical path of the light ray that exits the object at a height z, which in general can be described by [Deans, 1983]

$$\overset{\vee}{f}_{\phi}(p,z)=\int_{C} f(x,y,z)dl\,. \tag{73}$$

Under the minimum refraction approximation, the path C described by a light ray would be very similar to a straight line, as can be seen in Fig. 71, and it is noteworthy to state that this situation can be obtained if the object is submerged in oil [Goodman, 1985]. In this case, the optical path can be interpreted as the parallel projection at an angle ϕ as described in Eq. (73):

$$\overset{\vee}{f}_{\phi}(p,z)=\int_{-\infty}^{\infty}\int_{-\infty}^{\infty} f(x,y,z)\delta(p-x\cos\phi-y\sin\phi)dxdy\,, \tag{74}$$

where z is constant and indicates the height at which the cut is done, or the plane that defines the slice of the object that will be reconstructed.

In order to obtain the projection from the optical field (Eq. 72), it is necessary to apply an indirect method because an optical detector such as a CCD camera would observe something proportional to the square module of the amplitude of the field, being the phase undetectable, so the projection would also be undetectable. There are several proposals to obtain a projection of the optic filed, such as the interferometric techniques, which basically consist in making an interference of the field that exits the object with a reference wave, from which an interference pattern is obtained. The phase information is obtained from this pattern with some phase extraction technique, such as the phase shifting interferometry introduced by Brunning [Bruning *et. al.*, 1974] or by the Fourier transform suggested by Takeda [Takeda *et al.*, 1982], among others [Meneses-Fabian *et. al.*, 2011]. This type of technique is known as interferometric tomography, and has been applied in the study of temperature gradients in flames [Braslavsky *et al.*, 1998], in radiators and electronic chips [Wu & He, 1999] or in the measurement of concentration profiles in layers formed in the boundaries of cathodes in an electrolytic cell of $ZnCl_2$ [Kujawinska & Kniazewski, 2006], and in the study of phase objects, such as glasses, oils, acetates [Philipp *et al.*, 1992]. Nevertheless, image processing was always necessary to increase the processing quantity and the retrieval time of the image. Moreover, with these methods, it is possible to only retrieve the information related with the slice function of the object, but not of any operation over it. An alternative to retrieve some operation of the slice function has been proposed by finding the angular derivative, being made using an ESPI system which is sensible out of the plane to obtain the difference between two adjacent projections [Meneses-Fabian *et. al.*, 2003]. There are also other proposals, such as the use of a 4*f* system to obtain the directional derivative of the slice function, using a square root filter to obtain the semi derivative of the field, and by using it, to obtain something proportional to the derivative of the parallel projection [Rodríguez-Zurita *et al.*, 1997]. In this article, the proposal consists in using the 4*f* system to obtain the Hilbert transform of the field to detect information of the phase and the parallel projection.

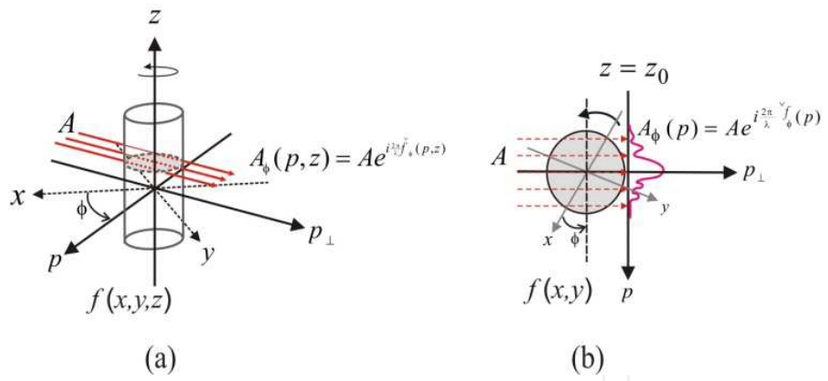

Fig. 7. Phase objects crossed by a plane wave, with a rotated reference system: (a) 3D object rotated around the *z* axis to generate the projection angle and (b) the slice of the object with *z* constant.

5.3.1.2 The Hilbert transform from the optical point of view

In this section, a tomographic system is proposed to detect the projection data from the irradiance, where the detection time for each projection data is reduced in time and cost. Moreover, not only are the projection data detected, but it is also possible to do an edge enhancement on the projection data emerging from the objects under study, and to retrieve the slice function of the object enhancing its characteristics, which cannot be detected with the unaided eye.

If the field that exits the object is considered as a function of the input transmittance of the image forming optical system, as schematically presented in Fig. 8, the field at the exit of the system is altered. The optical correlator consists of three planes and two lenses with the same focal distance *f*. As can be seen in Fig. 8, the distance between one lens and the adjacent plane is the focal distance of the lens *f*. The input plane is known as the object plane. The first lens finds the optical Fourier transform of the input field and this distribution is obtained in the Fourier plane. The second lens finds the optical Fourier transform in the Fourier plane, and distributes it in the output plane, known as the image plane. Then, at the exit of the system, we have the transform of the Fourier transform of the input transmittance function, which is the same function as the input, but inverted. Since it has also been convened that it is necessary to invert the axes in the image plane, the second lens makes the inverse Fourier transform. If a pupil function is placed on the Fourier plane, also known as frequency space filter, the exit function is the convolution of the input function with the result of the impulse of the filter [Abhilash, 2006]. In this case, the filtered used is a phase step of π radians, which is made depositing over one half of a slide a thin metallic layer calculating its thickness to provoke an expected delay for the wavelength used. The filter can be modeled by the *signum* function, and without loss of generality, the filter function can be written as

$$\tilde{h}_\phi(w,\zeta) = -i\,\mathrm{sgn}(w), \tag{75}$$

where ζ is the spatial frequency variable of *z*. In this manner, the optical field at the exit of the system can be mathematically described as

$$\overset{\frown}{A}_{\phi}(p,z)=\frac{\delta(z)}{\pi p}\otimes\otimes A_{\phi}(p,z), \tag{76}$$

which is the partial Hilbert transform respect to p of the input transmittance function, where it has been assumed that the relation $\delta(z)/\pi p=\Im^{-1}\{-i\,\mathrm{sgn}(w)\}$ is the response of the system. In what respects to the detection of the field, it is only possible to observe its irradiance, because an optical detector such as a CCD camera is used,

$$I_{\phi}(p,z)=\left|\frac{\delta(z)}{\pi p}\otimes\otimes A_{\phi}(p,z)\right|^{2}=\frac{\delta(z)}{\pi p}\otimes\otimes A_{\phi}(p,z)\left[\frac{\delta(z)}{\pi p}\otimes\otimes A_{\phi}^{*}(p,z)\right], \tag{77}$$

the symbol "*" indicates the complex conjugate. In the following sections, it will be shown how this intensity can be used to obtain the Hilbert transform of the projection data under the approximation of thin phase objects, and in the case of thick phase objects, it will be shown that this irradiance is taken directly as projection data, to reconstruct tomographic images with directional and isotropic edge-enhancement, respectively.

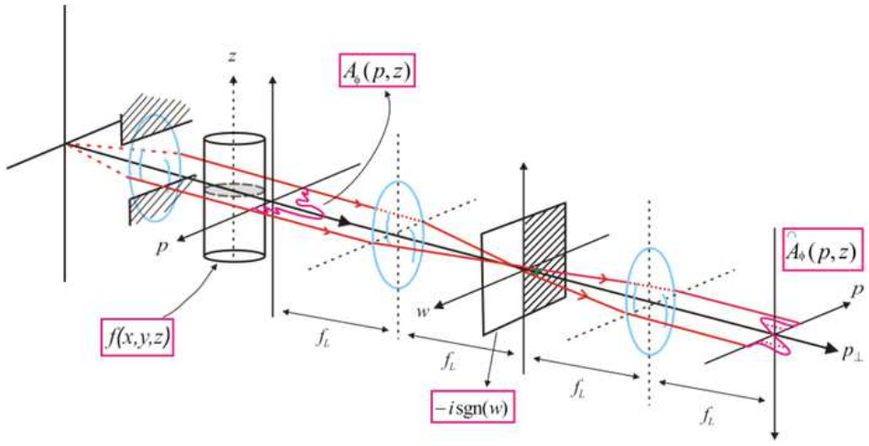

Fig. 8. Optical 4*f* image forming system

5.3.2 Edge-enhancement in optical tomography

5.3.2.1 Thin phase objects

In the thin phase object approximation, the exponential in Eq. (72) expresses the optical field that exits the object, and it is approximately equal to the initial terms of the Taylor series [Zernike, 1955], which is given by

$$A_{\phi}(p,z)=1+i\frac{2\pi}{\lambda}\overset{\vee}{f}_{\phi}(p,z), \tag{78}$$

where for the sake of simplicity, the amplitude of the field A has been approximated to 1. Substituting Eq. (72) in Eq. (78), the field exiting the system is given by:

$$\overset{\frown}{A}_{\phi}(p,z)=H^{0}\left\{1+i\frac{2\pi}{\lambda}\overset{\vee}{f}_{\phi}(p,z)\right\}=i\frac{2\pi}{\lambda}\overset{\frown}{\overset{\vee}{f}}{}^{0}_{\phi}(p,z), \tag{79}$$

where it has been assumed that $H\{1\}=0$. This equation indicates that the Hilbert transform of the field that is exiting the object is proportional to the Hilbert transform of the projection data for every height z, while its irradiance is expressed by:

$$I_{\phi}(p,z)=\frac{4\pi^2}{\lambda^2}\left(\overset{\cap}{\underset{\vee}{f}}{}_{\phi}^{0}(p,z)\right)^2. \tag{80}$$

In this manner, it is possible to obtain the module of the Hilbert transform of the projection, using:

$$\left|\overset{\cap}{\underset{\vee}{f}}{}_{\phi}^{0}(p,z)\right|=\frac{\lambda}{2\pi}\sqrt{I_{\phi}(p,z)}\,, \tag{81}$$

where the bars indicate absolute value. It is important to mention that the field at the exit of the system is proportional to the directional Hilbert transform of the input field with respect to p. Once a slice with height z has been selected, the Hilbert transform of the parallel projection at an angle ϕ is given. If this modified projection were extracted from the image plane, the reconstruction obtained would be extracted with the theory that is presented in section 5. But since this field is observed with a detector such as a CCD camera, then the result obtained would be proportional to the module of the Hilbert transform of the projection.
In order to validate the data indicated in Eq. (81) as projection data, it is necessary to use two properties of the Radon transform. In the case of the symmetry property,

$$\left|\overset{\cap}{\underset{\vee}{f}}{}_{\phi+\pi}^{0}(p,z)\right|=\left|\overset{\vee}{f}{}_{\phi+\pi}^{0}(p,z)\otimes\otimes\frac{\delta(z)}{\pi p}\right|=\left|-\overset{\vee}{f}{}_{\phi}^{0}(-p,z)\otimes\otimes\frac{\delta(z)}{\pi(-p)}\right|, \tag{82}$$

where it has been substituted in the symmetry property of the projection (Eq. 1). The first negative sign on the right-handed side of this equation can be eliminated for the sake of convenience due to the presence of the bars, so

$$\left|\overset{\cap}{\underset{\vee}{f}}{}_{\phi+\pi}^{0}(p,z)\right|=\left|\overset{\vee}{f}{}_{\phi}^{0}(-p,z)\otimes\otimes\frac{\delta(z)}{\pi(-p)}\right|=\left|\overset{\cap}{\underset{\vee}{f}}{}_{\phi}^{0}(-p,z)\right|, \tag{83}$$

which proves this property. For the zero momentum property, it is possible to state that

$$\int_{-\infty}^{\infty}dp\left|\overset{\cap}{\underset{\vee}{f}}{}_{\phi}^{0}(p,z)\right|=\int_{-\infty}^{\infty}dp\left|\overset{\vee}{f}{}_{\phi}^{0}(p,z)\otimes\otimes\frac{\delta(z)}{\pi(p)}\right|. \tag{84}$$

What lies in the parallel bars is the Hilbert transform of the projection for any height z. Nevertheless, it has been proved in section 6.2 that the zero momentum for this function is

null (Eq. 61). Therefore, in general, the area under the curve in the ranges in which the function is greater or equal to zero is identical to the area under the curve for the ranges in which the function is negative. This means that the positive area is equal to the negative, being the total area equal to zero. An intuitive proof of the fact that the areas in Eq. (84) remains constant, independently of how the projection angle is oriented, in the sense o the energy captured by the detector. Since the filter used in the Fourier plane of the 4*f* system has only one phase, this implies that there is no change in the energy of the light wave at the exit in the image plane when compared with the input in the object plane. Therefore, the irradiance in both the object plane, as well as in the image plane, is conservative. Hence, it is possible to intuitively conclude that the zero momentum of the Radon transform is satisfied for the projection that was obtained from the absolute value of the Hilbert transform of the projection. A more formal demonstration of this property remains beyond the purpose of this chapter.

Let us suppose that the slice function $f(x,y)$ with a rectangular domain in the way defined in Fig. 4a is shown in Fig. 9a1. The accumulated optical path of a light beam that crosses this slice $\overset{\vee}{f}_{\phi}(p)$ is calculated using the projection integral for different angles in the range $\phi \in (0,2\pi)$, in the way explained in section 6.3.1.1. The image obtained is shown in Fig. 9a2. The column (b) of this figure shows the optical field $A_{\phi}(p)$ that exits the slice of the object $f(x,y)$. The real and imaginary parts are shown in Fig. 8b1 and 8b2, respectively. The column (c) present the Hilbert transform of the field that exits the slice of the object. The real and imaginary parts are in Fig. 9c1 and 9c2, respectively. The upper row of the following column show the irradiance of $\overset{\frown}{A}_{\phi}(p,z)$, which is considered as a modified sinogram: a Hilbert-sinogram of the irradiance. In Fig. 9d2, the zero momentum of the Radon for the HIS is presented. It is important to note that the symmetry property and the zero momentum of the Radon transform are demonstrated, as was expected. Under the filtered retroprojection algorithm, the tomographic reconstruction is obtained. Fig. 9e shows the reconstruction obtained in 2D and 3D. In this algorithm, the rectangular filter is used, while the impulse response to this filter is used to filter the projection data using a numerical convolution.

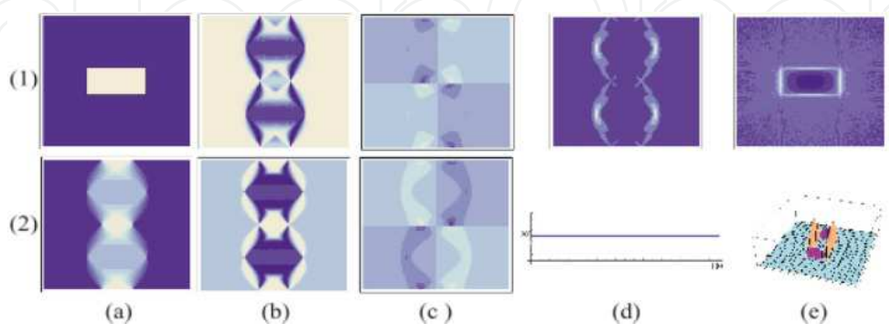

Fig. 9. Numerical simulation: (a) slice of the object (1) and sinogram (2); (b) field exiting the slice of the object: real (1) and imaginary (2); (c) Hilbert transform exiting the slice of the object, (d) Hilbert-sinogram of the irradiance (1) zero momentum of the Radon transform (2); and (e) reconstruction of the edge enhancement: en 2D (1) and 3D (2).

5.3.2.2 Thick phase objects

In the last section, the application of the tomographic theory of edge enhancement to thin phase objects was presented, where the first two terms in the Taylor series were used. In this section, the thick phase objects are considered, in which the field that exits the object cannot be approximated with only a few terms of the series. In this case, the irradiance of the partial Hilbert transform respect to p of the field that goes out of the object is considered as the projection data and it is proven that these data satisfies the two properties of the Radon transform required for the reconstruction of a slice function.
As was mentioned before, a CCD camera would observe the irradiance of the field existent in the image plane of the 4*f* system, as indicated in Eq. (80), which is now considered as the projection data:

$$I_\phi(p,z)=\left|\overset{\frown}{A}_\phi(p,z)\right|^2=\overset{\frown}{A}_\phi(p,z)\overset{\frown}{A}_\phi^*(p,z). \tag{85}$$

which satisfies the symmetry property. Now, let us verify this in the image plane, where the field is described by Eq. (76):

$$\overset{\frown}{A}_{\phi+\pi}(p,z)=\frac{\delta(z)}{\pi p}\otimes\otimes A_{\phi+\pi}(p,z)=\frac{\delta(z)}{\pi p}\otimes\otimes A_\phi(-p,z)=-\overset{\frown}{A}_\phi(-p,z). \tag{87}$$

The negative sign in the last term indicates that the partial Hilbert transform respect to p of the field at the exit of the object does not satisfy the property. Similarly, for the conjugated amplitude, it is possible to prove it:

$$\overset{\frown}{A}_{\phi+\pi}^*(p,z)=-\overset{\frown}{A}_\phi^*(-p,z). \tag{88}$$

Finally, for the irradiance in the image plane (Eq. 85), we have

$$I_{\phi+\pi}(p,z)=\overset{\frown}{A}_{\phi+\pi}(p,z)\overset{\frown}{A}_{\phi+\pi}^*(p,z)=\left[-\overset{\frown}{A}_\phi(-p,z)\right]\left[-\overset{\frown}{A}_\phi^*(-p,z)\right]=I_\phi(-p,z), \tag{89}$$

which proves the property. For the zero momentum of the Radon transform,

$$\int_{-\infty}^{\infty}dpI_\phi(p,z)=\int_{-\infty}^{\infty}dp\,\overset{\frown}{A}_\phi(p,z)\overset{\frown}{A}_\phi^*(p,z). \tag{90}$$

Applying Parseval's theorem,

$$\int_{-\infty}^{\infty}dpI_\phi(p,z)=\int_{-\infty}^{\infty}dw\,\overset{\sim}{\overset{\frown}{A}}_\phi(w,z)\overset{\sim}{\overset{\frown}{A}}_\phi^*(w,z)=\int_{-\infty}^{\infty}dw\left[-i\,\mathrm{sgn}(w)\,\tilde{A}_\phi(w,z)\right]\left[i\,\mathrm{sgn}(w)\,\tilde{A}_\phi^*(w,z)\right], \tag{91}$$

where it has been assumed that $\overset{\sim}{\overset{\frown}{A}}_\phi(w,z)=-i\,\mathrm{sgn}(w)\,\tilde{A}_\phi(w,z)$ is the partial Fourier transform respect to p of the field in the image plane of the 4*f* system, and $A_\phi(w,z)=\Im\{A_\phi(p,z)\}$ is the partial Fourier transform respect to p of the field that exits the object. Accepting the identity $\mathrm{sgn}^2(w)=1$, it is possible to simplify this expression, resulting in:

$$\int_{-\infty}^{\infty} dpI_{\phi}(p,z) = \int_{-\infty}^{\infty} dw\, \tilde{A}_{\phi}(w,z)\, \tilde{A}_{\phi}^{*}(w,z), \tag{92}$$

and by using again Parseval's theorem, Eq. (92) can be written in the following way:

$$\int_{-\infty}^{\infty} dpI_{\phi}(p,z) = \int_{-\infty}^{\infty} dpA_{\phi}(p,z)A_{\phi}^{*}(p,z)\,. \tag{93}$$

This expression states that the intensity of the object plane and in the image plane are the same, which is consistent, due to the fact that the filter used has only one phase. Now, if Eq. (72) is substituted in Eq. (93), the following expression is finally obtained:

$$\int_{-\infty}^{\infty} dpI_{\phi}(p,z) = \int_{-\Gamma/2}^{\Gamma/2} dpA \exp\left[i\frac{2\pi}{\lambda} \overset{\vee}{f}_{\phi}(p,z)\right] A \exp\left[-i\frac{2\pi}{\lambda} \overset{\vee}{f}_{\phi}(p,z)\right] = A^2\Gamma\,, \tag{94}$$

where Γ is the width of the detector, where the irradiance is zero outside of this width. Considering the irradiance in the image plane as the projection data, the zero momentum of the Radon transform is the total energy in the finite detector, and is independent of ϕ. Therefore, the symmetry property and the zero momentum of the Radon transform have been proved in a satisfactory way, so the irradiance in the image plane can be considered as the projection data, and thus, the tomographic reconstruction must present a consistent image.

In Fig. 10, there are two examples: in the row 1, a uniform ring is considered as the slice of the object, and in row 2, a non-symmetrical slice of the object is considered as the slice of the object. In column (a), we present the slices of the object. The set of data in the image plane for every possible projection angle form a modified sinogram known here as a Hilbert-sinogram of the irradiance (HIS) is displayed in column (b). In column (c), the zero momentum of the Radon transform is displayed, and finally, in columns (d) and (e), both of the reconstructions in 2D and 3D are presented, respectively.

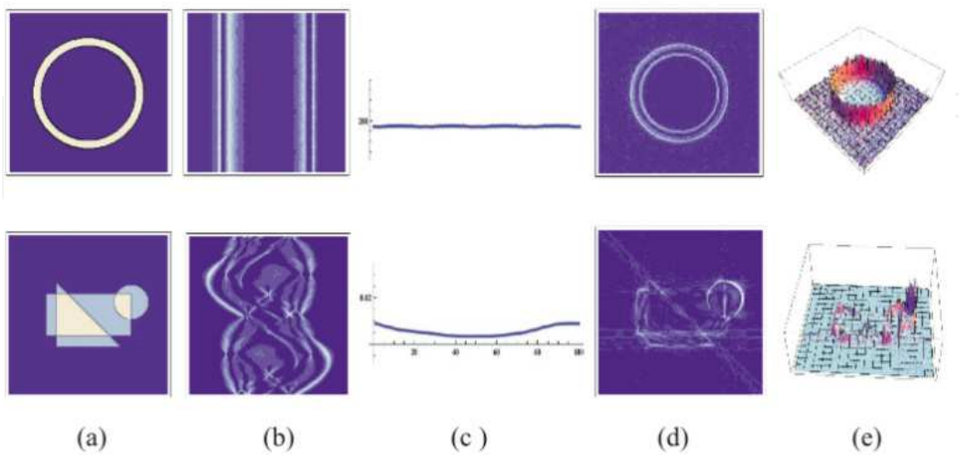

Fig. 10. Numerical simulation: (a) Two test slices: a uniform ring and a non-uniform object, (b) HIS; (c) the zero momentum of the Radon transform (2); (d, e) the reconstruction of the edge enhancement in 2D (1) and 3D (2).

The irradiance in the image plane of the 4*f* optical system using a phase filter of π radians has been considered as the projection data in optical tomography of phase objects, and this has been mathematically demonstrated, that the irradiance satisfies the symmetry property, as well as with the zero momentum of the Radon transform. It has been proven that for every possible projection angle, it is possible to obtain a modified sinogram, which is called a Hilbert-sinogram of the irradiance. As a consequence of the direct use of this HIS, the reconstruction obtained consists of images that show an isotropic edge enhancement for the numerical simulation. Thus, the filtered Hilbert transform not only serves to detect the phase projections, but it also is capable to reinforce tomographic images as an additional characteristic.

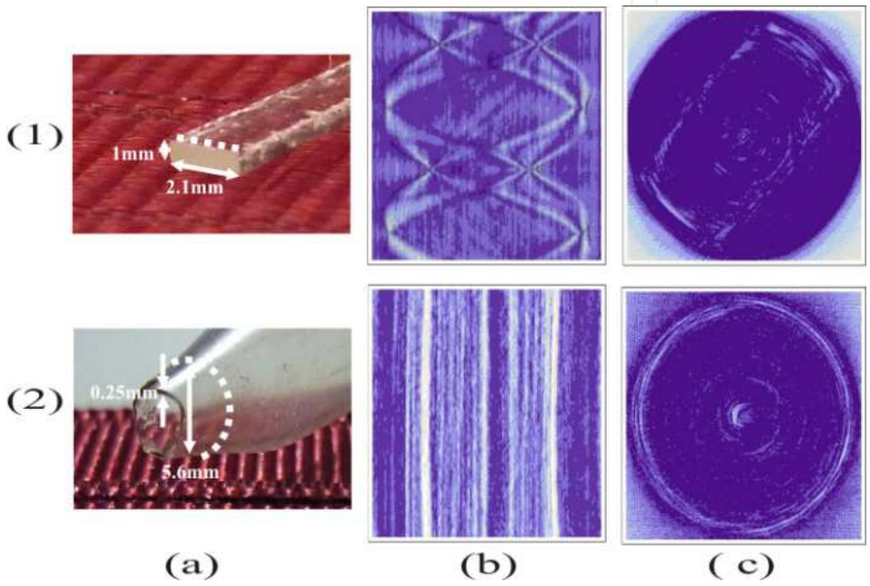

Fig. 11. Experimental results: (a1) a rectangular piece, (a2) pipette, both made of Pyrex, with a refraction index of 1.52; (b) their respective Hilbert-sinogram of irradiance obtained experimentally; and (c) the reconstruction of a slice of the object, respectively for each of the objects under study, where the slice is indicated by the dotted line in (a).

5.3.2.3 Experimental results

In this section, the experimental results for the tomography of phase objects with an isotropic edge enhancement are presented. The 4*f* system shown in Fig. 8 is a telecentric system that can be implemented in laboratory table, in order to achieve the optical phase object tomography. In the experimental implementation, the lenses used have a focal distance of $f_L = 479mm$; the step filter of π radians was found adequate for the wavelength used of $\lambda = 632.8nm$. In the experimental setup, the object under study is submerged on one of its ends in a liquid opening with immersion oil. This oil has a nominal index of 1.515. In this manner, the refractional limit condition is satisfied, while the other end is suspended by the axis of a step-wise motor, with a resolution of 1.8^o for every step, which is controlled by a program designed in LabVIEW with an interface for a PC, which also controls the CCD camera, and selects the line of interest in the object, defining the slice of the object.

With this experimental array, and with the control managed from the PC, it is possible to place the sample at the desired projection angle. In the initial position of the sample, it is considered in a rectangular coordinate system, which rotates around the z axis, and where ϕ is the azimuthal rotation angle respect to the x axis, for z constant. In order to experimentally obtain the Hilbert-sinogram of the irradiance, the CCD camera is placed in the image plane of the 4*f* system and is controlled through the visual interface, synchronizing the acquisition of the projection data. In order to obtain the retroprojection data that will form the Hilbert sinogram of the irradiance, it is necessary to select a data line, and it is maintained fixed during the acquisition of all the projections. In the initial position of the object, it is considered that $\phi = 0$ as the first projection angle. The data observed in this row in the image plane using the CCD camera are placed in the new image where the Hilbert-sinogram of the irradiance will be constructed. Once these procedure has been finished, the step-wise motor rotates the sample one step of 1.8º, generating a second projection angle, and it is noteworthy to state that due to this rotation, the distribution of the field has been modified. Once again, the same row of data is selected to be observed by the CCD camera and they are arranged in the second row of the image where the Hilbert-sinogram of the irradiance is being constructed. Repeating this for each one of the angular steps of the motor until a complete rotation of 360º has been accomplished, the Hilbert-sinogram of irradiance has been completely constructed for one slice of the object, so this will have 200 rows. The reconstruction of the slice with an isotropic edge-enhancement is obtained submitting the HIS to data processing, using the filtered retroprojection. It is important to state that due to the symmetry property of the parallel projections, it was only necessary to use the projections that lie in the range $(0^0, 180^{0'})$.

In Fig. 11, there are experimental results for two phase objects. Fig. 11a presents the photographs of the transparent objects that were studied. The sample number 1 is an object that is a rectangular piece of 1x3x20 mm, (1) a pipette of 5.6 mm of external diameter and 0.25 mm of thickness. Both objects are made of Pyrex glass with a nominal refraction index of 1.52. Fig. 11b show the HIS experimentally obtained of a slice of each one of the objects. The slices that were selected for each one of the objects are shown in Fig. 11a by a dotted line. Fig. 11c presents their respective tomographic reconstruction using the filtered retroprojection algorithm. The tomographic images that were obtained show edge enhancement. These enhancements are related principally to the refraction index over some slice in particular.

6. Conclusions

In this chapter, there was a discussion of the mathematical fundamentals of parallel projection tomography, and there was also a demonstration of the mathematical method for directional edge-enhancement tomography. It is important to state that this technique is possible thanks to the mathematical relationship existent between the Radon transform and the Hilbert transform. Numerical simulations were done, and it was proven how this technique can be applied in phase object tomography, presenting reconstructed images with isotropic edge enhancement. Note that an analytic proof of the isotropic edge enhancement continues being an open problem.

Three conditions were required in order to make possible the implementation of the edge-enhancement tomography:

1. The existence of a relationship between the Hilbert transform and the Radon transform.
2. The verification of the symmetry property and the zero momentum of the Radon transform of the Hilbert transform of the projections.
3. The possibility of an experimental implementation of the Hilbert transform

Due to its analytic form, the third one can be implemented in an invariant and linear system because the spectrum is the product of two functions in Fourier-space, where one of the functions can be interpreted as the filter function. This is why the optical implementation of the Hilbert transform is possible, where the step phase filter is used because it is modeled through the *signum* function. Moreover, in terms of detection, this method is more direct and faster than the usual methods used in interferometric tomography, because there is no data preprocessing implied in the obtaining of the projection data.

Speaking in general terms, this same detection method could be extended using another type of filter that can make edge-enhancement, such as the full or fractional directional derivative. This technique could be employed using another type of probe that can make possible the implementation of a linear and invariant system. We think that the tomography through electric capacitance can be done in this way, because it is possible to implement a system of this type, in the way done in communication systems.

7. Acknowledgment

This work was partially supported by PROMEP under grant PROMEP/103.5/09/4544 and by Vicerrecoría de Investigación y Estudios de Posgrado under grant MEFC.

8. References

Abhilash, G., (2006). Hilbert transform: A simple, signal-theoretic formulation, *Article series of the Signals Research Laboratory*

Almeida, L.B., (1994). The fractional Fourier transform and time-frequency representation. IEEE Trans. Sig. Proc., 42:3084–3091

Andersen, A. H. and Kak, A. C., (1982). Digital ray tracing in two-dimensional refractive fields, *Journal of the Acoustical Society of America*, Vol. 72, pp. 1593-1606

Baba, N. and Murata, K., (1977). Filtering for image reconstruction from projections, *Journals Optics Society America*, pp.662-668

Bates, R. H. T. and Peters, T. M., (1983). Overview of computerized tomography with emphasis on future developments, *Proceedings IEEE*, Vol. 71, pp. 356-372

Bracewell, R. N. and Riddle, A. C., (1967). Inversion of fan-beam scans in radio astronomy, *The Astrophysical Journals*, Vol.150, pp. 427-434

Bracewell, Ronald N.; McGraw-Hill (2000). *The Fourier transform and its application*, Stanforf University

Bracewell, R. N., (1956). Strip integration in radio astronomy, *Australian Journal of Physics*, Vol. 9, pp. 198-217

Braslavsky, I. and Lipson Technion, S. G., (1998). Interferometric Tomography Measurement of the Temperature Field in the Vicinity of a Dendritic Crystal Growing from a

Supercooled Melt. Transactions of Optical methods and data processing in heat and fluid flow, IMECHE, London, pp. 423-432.

Brown, W. P., Jr., (1966). Validity of the Rytov Approximation in Optical Propagation Calculations. *Journals Optics Communications*, Vol. 56, pp.1045-1052

Bruning, J. H., Herriott, D.R., Gallagher, J. E., Rosenfeld, D. P., White, A. D., and Brangaccio, D. J., (1974). Digital Wavefront Measurement Interferometer for Testing Optical Surfaces and Lenses, Applied Optics, Vol. 13, pp. 2693

Byer, R. L., Garbuny, M., (1973). Pollutant detection by absorption using Mie scattering and topographic targets as reflectors, *Applied Optics,* Vol. 12, No.7, pp. 1496-1505

Byer, R. L., Shepp, L. A., (1979). Two-dimensional remote air-pollution monitoring via tomography, *Optics Letters*, Vol.4, pp. 375-377

Chiu, M. Y., Barrett, H. H., Simpson, R. G., Chou, C., Arendt, J. W., and Gindi, G. R., (1979). Three dimensional radiographic imaging with a restricted view angle, *Journal of the Optical Society of America* ,Vol. 69, pp. 1323-1330

Chiu, M. Y., Barrett, H. H., Simpson, R. G., (1980). Three dimensional reconstruction from planar projections, *Journal of the Optical Society of America*, Vol. 70, pp. 755-762

Davis, Jeffrey A. and Nowak, Maria D., (2001). Selective edge enhancement of images with an acousto-optic light modulador, *Applied Optics*, Vol. 23, pp. 4835-4839

Davis, Jeffrey A., McNamara, D. E., Cottrell, D. M., and Campos, J., (1998). Analysis of the fractional hilbert transform, *Applied Optics*, Vol. 37, pp. 6911-6913

Davis, Jeffrey A., McNamara, D. E., Cottrell, D. M., and Campos, J., (2000). Image processing with the radial Hilbert transform: theory and experiments, *Optics Letters*, Vol. 25, pp.99-101

Davis, Jeffrey A., and Nowak, M. D., (2002). Selective-edge enhancement of images with an acousto-optic light modulator, *Applied Optics*, Vol. 41, pp. 4835-4839

Deans, Stanley R.; John Wiley & Sons (1983). *The Radon Transform and Some of its Applications,* New York

DeRosier, D. J. and Klug, A., (1968). Reconstruction of three dimensional structures from electron micrographs, *Nature*, Vol. 217, pp. 130-134

Eden, O. Tretiak. M., and Simen, M., (1969). International structures dor three dimensional images, in *Proc. 8th Int. Conference on Medicine Biological Engineering, Chicago, IL*

Fatemi, M. and Kak, A. C., (1980). Ultrasonic B- scan imaging: Theory of image formation and a technique for restoration, *Ultrasonic Imaging on ScienceDirect*, Vol. 2, pp. 1-47

Glover, G. H., (1982). Compton scatter effects in CT CT reconstructions, *Medical Physics*, Vol. 9, pp. 860-867

Goodman, Jooseph W.; J. Wiley & Sons (1985). *Introduction to Fourier optics*

Haykin, S., Ed. Englewood Cliffs, NJ; Prentice-Hall (1985). *Tomographic imaging with diffracting and non-diffracting sources, in Array Signal Processing*

Herman, G. T. and Naparstek, A., (1977). Fast image reconstruction based on a Radon inversion formula appropriate for rapidly collectes data, *SIAM Journals on Applied Mathematics*, Vol. 33, pp. 511-533

Horn, B. K. P., (1978). Density reconstruction using arbitrary ray sampling schemes, *Proccedings of the IEEE*, Vol. 66, pp. 551-562

Horn, B. K. P., (1979). Fan-beam reconstruction methods, *Proccedings of the IEEE*, Vol. 67, pp. 1616-1623

Hsu, Hwei P.; Addison-Wesley Iberoamericana (1970). *Analisis de Fourier*, Nueva York

Kak, A. C., Slaney, M.; New York (1987). *Principles of Computarized Tomographic Imaging*, IEEE Press

Kenue, S. K. and Greenleaf, J. F., (1979). Efficient convolution kernels for computerized tomography, *Ultrason Imaging*, Vol. 1, pp.232-244

Kenue, S. K. and Greenleaf, J. F., (1979). Efficient convolution kernels for computerized tomography, *Ultrason Imaging*, Vol. 1, pp.232-244

Kujawinska, Malgorzata, Kniazewski, Pawel, (2006). Enhanced interferometric and photoelastic tomography for 3D studies of phase photonics elements, Proceedings of the Symposium on Photonics Technologies for 7th Framework Program Wroclaw 12-14 October, pp. 467-471

Kwoh, Y. S., Reed, I. S., and Truong, T. K., (1977). A generalized $|w|$-filter for 3-D reconstruction, *IEEE Transactions on Nuclear Science*, Vol. NS-24, pp. 1990-1977

Lakshminarayanan, A. V., (1975). Reconstruction from divergent ray data, Tech. Rep. 92, Dep. Of Computer Science, State Univ. of New York at Buffalo

Lewitt, R. M. and Bates, R. H. T., (1978). Image reconstruction from projections, *Optik*, Vol. 50, pp. 19-33

Lewitt, R. M., (1979). Ultra-fast convolution approximation for computerized tomography, *IEEE Transactions on Nuclear Science*, Vol. NS-26, pp. 2678-2681

Meneses-Fabian, Cruz, Montes-Perez, Areli, and Rodriguez-Zurita, Gustavo, (2011). Directional edge enhancement in optical tomography of thin phase objects, *Optics Express*, Vol. 19, pp. 2608-2618

Meneses-Fabian, Cruz, Rodriguez-Zurita, Gustavo, Rodriguez-Vera, Ramon, Vazquez-Castillo, Jose F., (2003).Optical tomography with parallel projection differences and Electronic Speckle Pattern Interferometry, Optics Communications, Vol. 228, pp. 201-210

Montes-Perez, Areli, Meneses-Fabian, Cruz, Rodriguez-Zurita, Gustavo, (2011). Optical Hilbert-transform to isotropic edge-enhancement in phase object tomography, *Optics Express*, Vol. 19, pp. 5350-5356

Oppenheim, B. E., Ter Pogossian, M. M. et. al., Eds. Baltimore, MD ; (1975). *Reconstruction tomography from incomplete projections, in reconstruction Tomography in Diagnostic Radiology and Nuclear Medicine*, University Park Press

Ornelas-Rodríguez, F.J., Rodríguez-Zurita, G., Rodríguez-Vera, R., Pastrana Sánchez , R., de la Rosa-Miranda, E., (1999). Zero-order moment of the Radon transform in tomography: some further remarks, Optics Communications, Vol. 161, pp. 19-24

Poularikas, A. D.; CRC PRESS, IEEE PRESS (2000). The transforms and applications handbook, United States of Ameirca

Philipp, H., Neger, T., Jäger, H. and Woisetschläger, J., (1992). Optical tomography of phase objects by holographic interferometry, Elsevier Ltd. Vol. 10, pp. 170-181

Ramachandran, G. N. and Lakshminarayanan, A. V., (1971). Three dimensional reconstructions from radiographs and electron micrographs: Application of convolution instead of Fourier transforms, *Proceedings of the National Academy of Sciences*, Vol. 68, pp. 2236-2240

Rodríguez-Zurita, G., Meneses-Fabián, C., Pérez-Huerta, J.-S., Vázquez- Castillo, J.-F., (2005). Tomographic directional derivative of phase objects slices using 1-D derivative spatial filtering of fractional order 1/2, *20th Congress of the International Commission for Optics*, *Proceedings SPIE*, Vol. 6027, pp. 0405-056

Rodríguez-Zurita, G. and Pastrana-Sánchez, R., (1997). Tomographyc phase-distribution edge enhancement with differences projectionsa proposal, 4 Revista Mexicana de Física, Vol. 43, pp. 167-174

Rowley, P. D., (1969). Quantitative interpretation of three dimensional weakly refractive phase objects using holographic interferometry, *Journal of the Optical Society of America*, Vol 59, pp. 1496-1498

Sato, T., Norton, S. J., Linzer, M., Ikeda, O., and Hirama, M., (1980). Tomographic image reconstruction from limited projections using iterative revisions in image and transform spaces, *Applied Optics*, Vol. 20, pp. 395-399

Seeley, R., Ed Reverte (1970). *Introducción a las Series e Integrales de Fourier*

Shepp, L. A. and Logan, B. F., (1974). The Fourier reconstruction of a head section, *IEEE Transactions on Nuclear Science*, Vol. NS-21, pp. 21-43

Smith, B. D., (1985). Image reconstruction from cone-beam projections; Necessary and sufficient conditions and reconstruction methods, *IEEE Transactions on Medical Imaging*, Vol. MI-4, pp. 14-25

Stark, H., Woods, J. W., Paul, I., and Hingorani, R., (1981). Direct Fourier reconstruction in computer tomography, *IEEE Transactions Acoustics and Speech Signal Processing*, Vol. ASSP-29, pp. 237-244.

Takeda, M., Ina, H., and Kobayashij, S., (1982). Fourier-transform method of fringe-pattern analysis for computer-based topography and interferometry, Optics Society American, Vol. 72, pp. 156-160

Tam, K. C. and Perez-Mendez, V., (1981). Tomographical imaging with limited angle input, *Journal of the Optical Society of America*, Vol. 71, pp. 582-592

Tanaka, E. and Iinuma, T. A., (1975). Correction functions for optimizing the reconstructed image in transverse section scan, *Physics in Medicine Biology*, Vol. 20, pp. 789-798

Vest, C. M., and Radulovic, P. T.; Pergamon (1977). *Measurement of three-dimensional temperature fields by holographic interferometry, in Applications of Holography and Optical Data Processing*, E. Marcom, A. A. Friesem, and E. Wiener-Avnear, pp. 241-249, Oxford

Wernecke, S. J. and D'Addario, L. R., (1977). Maximum entropy image reconstruction, *IEEE Transactions Computers*, Vol. C-26, pp. 351-364

Wolf, E., (1969). Three-dimensional structure determination of semi-transparent objects from holographic data. *Optics Communications*, Vol.1, pp.153-156

Wu, Donglou and He, Anzhi, (1999). Measurement of three-dimensional temperature fields with interferometric tomography, Applied Optics, Vol. 38, pp. 3468 -3473

Zernike, F., (1955). How I discovered phase contrast, *Science*, Vol. 121, pp. 345-349

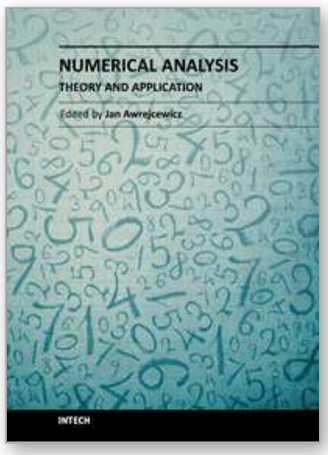

Numerical Analysis - Theory and Application

Edited by Prof. Jan Awrejcewicz

ISBN 978-953-307-389-7
Hard cover, 626 pages
Publisher InTech
Published online 09, September, 2011
Published in print edition September, 2011

Numerical Analysis â€“ Theory and Application is an edited book divided into two parts: Part I devoted to Theory, and Part II dealing with Application. The presented book is focused on introducing theoretical approaches of numerical analysis as well as applications of various numerical methods to either study or solving numerous theoretical and engineering problems. Since a large number of pure theoretical research is proposed as well as a large amount of applications oriented numerical simulation results are given, the book can be useful for both theoretical and applied research aimed on numerical simulations. In addition, in many cases the presented approaches can be applied directly either by theoreticians or engineers.

InTech Europe
University Campus STeP Ri
Slavka Krautzeka 83/A
51000 Rijeka, Croatia
Phone: +385 (51) 770 447
Fax: +385 (51) 686 166
www.intechopen.com

InTech China
Unit 405, Office Block, Hotel Equatorial Shanghai
No.65, Yan An Road (West), Shanghai, 200040, China
中国上海市延安西路65号上海国际贵都大饭店办公楼405单元
Phone: +86-21-62489820
Fax: +86-21-62489821

IntechOpen